The GFDL Cloud Microphysics Parameterization

Linjiong Zhou
Princeton University

Lucas Harris
NOAA/Geophysical Fluid Dynamics Laboratory

Jan-Huey Chen
University Corporation for Atmospheric Research,

NOAA/Geophysical Fluid Dynamics Laboratory

1 July 2022
Document Version 4.0

Contents

1   Introduction

Clouds play critical roles in our daily weather and in the global energy and water budgets that regulate the climate of the Earth (Lamb and Verlinde, 2011; Houze, 2014). The formation and evolution of clouds significantly impact precipitation forecasts in numerical weather prediction (Seifert and Beheng, 2005; Morrison and Grabowski, 2008; Baldauf et al., 2011; Bauer et al., 2015). Clouds and their impacts on solar and thermal radiation are among the most challenging aspects of climate prediction (Trenberth et al., 2009; Stephens et al., 2012; Wild et al., 2019). Therefore, the representation of clouds in atmospheric models has to be paid particular attention to. Among all physical processes in a model, cloud microphysics is less well represented but is of critical importance. Because the processes are not readily resolved in time and space, cloud microphysics parameterization is essential from large-eddy to global simulations (Morrison and Grabowski, 2008; Kogan, 2013; Nogherotto et al., 2016).

1.1   History

Two cloud microphysics schemes have been developed at the Geophysical Fluid Dynamics Laboratory (GFDL) for use in global climate and weather models. One is the Rotstayn-Klein cloud microphysics scheme (Rotstayn, 1997; Klein and Jakob, 1999; Rotstayn et al., 2000; Jakob and Klein, 2000); the other one is a single-moment five-category cloud microphysics scheme (Chen and Lin, 2011, 2013; Zhou et al., 2019; Harris et al., 2020; Zhou et al., 2022). This document focuses on the latter one. The single-moment five-category cloud microphysics scheme (GFDL MP for short hereafter) was developed based on the Lin-Lord-Krueger cloud microphysics scheme (Lin et al., 1983; Lord et al., 1984; Krueger et al., 1995) formerly used in the GFDL ZETAC regional model (Pauluis and Garner, 2006; Knutson et al., 2007, 2008). It was substantially revised and redesigned by Dr. Shian-Jiann Lin for the GFDL global high-resolution model HiRAM (High-Resolution Atmospheric Model) in the early 2000s (Zhao et al., 2009; Chen and Lin, 2011, 2013; Harris et al., 2016; Gao et al., 2017, 2019). This version can be called as GFDL MP version 0 (GFDL MP v0). It is being continually developed and maintained by the FV3 team for various applications ranging from convective-scale to seasonal-scale prediction, from regional to global domains. We released GFDL MP v1 as in (Zhou et al., 2019), and GFDL MP v2 as in Harris et al. (2020). In addition, for climate and very-long-time simulation, it is widely recognized that a double-moment scheme (or other added complexity schemes such as triple-moment or spectral bin schemes) can improve the representation of clouds and cloud feedbacks (Reisner et al., 1998; Swann, 1998; Luo et al., 2008; Morrison et al., 2009; Dawson et al., 2010; Milbrandt and McTaggart-Cowan, 2010; Jung et al., 2012; Molthan and Colle, 2012; Van Weverberg et al., 2012; Baba and Takahashi, 2014; Jin et al., 2014; Igel et al., 2015). Therefore, the GFDL MP was rewritten entirely in early 2021 to allow the future development of the double-moment capability for climate simulation and the weather to seasonal prediction (Zhou et al., 2022). This version can be called as GFDL MP v3. This document has been updated to represent the GFDL MP v2 that was briefly described in Harris et al. (2020). The latest development in GFDL MP v3 described in Zhou et al. (2022) will be included in the next release of this document.

1.2 Features

The GFDL MP was designed to be integrated within the Finite-Volume Cubed-Sphere Dynamical Core (FV3), thus it has the following featured attributes that are more or less originated from the FV3 (Zhou et al., 2019; Harris et al., 2020). The first feature is inline cloud microphysics. All cloud processes are embedded within the Lagrangian-to-Eulerian remapping in the FV3 dynamical core and can be updated more frequently than the rest of the physics. The second feature is fast and stable sedimentation. Time-implicit monotonic scheme and piecewise parabolic method are applied to falling condensates, ensuring shape preservation and stability without subcycling (see section 4). The third feature is consistent thermodynamics. Thermodynamic consistency is maintained between the dynamics and the physics by considering the heat content of the condensates. As a result, the total moist energy is precisely conserved within the cloud microphysics scheme (see section 2). The fourth feature is sedimentation effect. Condensates carry heat and momentum during the sedimentation processes (see section 4). The fifth feature is scale awareness. Scale awareness is achieved by an assumed horizontal subgrid variability and a second-order finite-volume-type vertical reconstruction for autoconversion processes (see section 2).

1.3 Application

The GFDL MP was originally developed within HiRAM as one of its essential components. HiRAM showed excellent performance in the convective-scale forecast, sub-seasonal to seasonal prediction, and climate simulation (Chen and Lin, 2011, 2013; Harris et al., 2016; Gao et al., 2017, 2019). This cloud microphysics scheme has also been an option of the GFDL modeling system suites for most 25-km resolution configurations and radiative-convective equilibrium (RCE) simulations (Jeevanjee, 2017; Jeevanjee and Zhou, 2022). In 2011, this cloud microphysics scheme has been adopted by the climate modeling system of the Institute of Atmospheric Physics (IAP) at the Chinese Academy of Sciences (CAS). The IAP / CAS model with this cloud microphysics scheme achieves excellent global energy and water balance, improved Madden-Julian Oscillation (MJO), and hurricane predictions (Zhou et al., 2015; Li et al., 2019; He et al., 2019). In 2016, the GFDL MP was implemented into the Next Generation Global Prediction System (NGGPS) to replace the current Zhao-Carr cloud microphysics scheme (Zhao and Carr, 1997). With this upgrade, the NGGPS significantly outperforms the "Legacy" Spectral Global Forecast System (GFS) in the global forecast skill (Zhou et al., 2019; Harris et al., 2020; Zhou et al., 2022) and hurricane prediction (Chen et al., 2019b,a). This model also shows skillful predictions of convective storms over the contiguous United States (Zhou et al., 2019; Harris et al., 2019). On June 12, 2019, the National Weather Service (NWS) upgraded its operational GFS to version 15 which included the FV3 dynamical core as well as the GFDL MP (https://www.emc.ncep.noaa.gov/gmb/STATS/html/model_changes.html). The most up-to-date GFS version 16 still adopts the GFDL MP since it helps to produce excellent forecasts. The NWS's Hurricane Analysis and Forecast System (HAFS) is also using this cloud microphysics scheme for hurricane predictions(Dong et al., 2020; Hazelton et al., 2021). More recently, the National Aeronautics and Space Administration (NASA) Goddard Earth Observing System Model, Version 5 (GEOS-5) adopted this cloud microphysics scheme in their cloud-resolving simulations (Arnold et al., 2020).

1.4   Structure

This document is organized as follows: Section 2 describes the basic theory of the cloud microphysics scheme, which includes basic equations, definition of meteorological fields, size distribution, subgrid variability, conversion rate, saturation water vapor pressure, and energy conservation. Section 3 describes all cloud microphysical processes, which includes saturation adjustment, accretion, autoconversion, freezing / melting, and others. Section 4 describes the equations to calculate sedimentation and precipitation. Section 5 describes some diagnosis outputs, which are cloud fraction, radar reflectivity, cloud effective radius. The appendices provide further information on symbols, constants used in this document, namelist of parameters, and update records.

2   Theory

2.1   Basic Equations

Like many other single-moment bulk cloud microphysics schemes (Rutledge and Hobbs, 1983, 1984; Cotton et al., 1986; Dudhia, 1989; Tao and Simpson, 1993; Walko et al., 1995; Thompson et al., 2004; Hong and Lim, 2006; Nogherotto et al., 2016), the GFDL MP consists of water vapor (q_{vapor}) and five categories of hydrometeors defined as the mass mixing ratio of cloud water (q_{water}), cloud ice (q_{ice}), rain (q_{rain}), snow (q_{snow}), and graupel or hail ($q_{graupel}$ or q_{hail}) and contains various processes to parameterize the conversions between them (Figure 1). As a single-moment cloud microphysics scheme, all other moments of the hydrometeor size distribution are prescribed or diagnosed. For example, the number concentration (zeroth moment) is prescribed as a constant for all categories of hydrometeors. The effective radius (third moment divided by second moment) and radar reflectivity (sixth moment) are diagnosed at the end of the cloud microphysics scheme.

The prognostic equations governing the mass mixing ratio conversion between hydrometeors shown in Figure 1 are written as:

$$
\begin{aligned}
\frac{\partial q_{vapor}}{\partial t} =& Pevap + Pisub + Prevp + Pssub + Pgsub \\
& - Pcond - Pidep - Psdep - Pgdep
\end{aligned}
\tag{2.1}
$$

$$
\begin{aligned}
\frac{\partial q_{water}}{\partial t} =& Pcond + \alpha Pimlt + \epsilon Psmlt + \epsilon Psacw + \epsilon Psacr + \epsilon Pracs \\
& - Pevap - Pifr - Pracw - Praut - Pgacw - Pcomp - Pbigg
\end{aligned}
\tag{2.2}
$$

$$
\begin{aligned}
\frac{\partial q_{ice}}{\partial t} =& Pidep + \beta Pifr + Pcomp + Pbigg \\
& - Pisub - Pimlt - Psaci - Psaut - Pgaci
\end{aligned}
\tag{2.3}
$$

$$
\begin{aligned}
\frac{\partial q_{rain}}{\partial t} =& Pracw + Praut + (1-\alpha)Pimlt + (1-\epsilon)Psmlt + Pgmlt + (1-\epsilon)Pascr \\
& + (1-\epsilon)Pracs + (1-\epsilon)Psacw + Pgacw + Pgacr \\
& - Prevp - Psacr - Pgacr - Pgfr
\end{aligned}
\tag{2.4}
$$

$$
\begin{aligned}
\frac{\partial q_{snow}}{\partial t} =& Psdep + (1-\beta)Pifr + Psaci + Psaut + Psacr \\
& - Pssub - Psmlt - Pracs - Pgacs - Pgaut - Psacw - Psacr
\end{aligned}
\tag{2.5}
$$

$$
\begin{aligned}
\frac{\partial q_{graupel}}{\partial t} =& Pgdep + Pgacw + Pgaci + Pgacr + Pgfr + Pgacs + Pgaut \\
& - Pgsub - Pgmlt - Pgacw - Pgacr,
\end{aligned}
\tag{2.6}
$$

where α, β, and ϵ represent the partitioning of $Pimlt$, $Pifr$, $Psmlt$, $Psacw$, $Psacr$, and $Pracs$ in separated microphysical processes. Note that all relevant hydrometeors and temperature are updated immediately after each cloud microphysical process based on exact mass conservation and moist total energy conservation. The meaning and source of each item on the right-hand side of Equations (2.1) to (2.6) and in Figure 1 are demonstrated in Table 1. Conversion between hydrometeors in different phases involves heating and cooling of the air, while that between hydrometeors in the same phases does not. Most of the microphysical processes, as well as the parameters, are revised from Lin et al. (1983); Hong et al. (2004); Hong and Lim (2006).
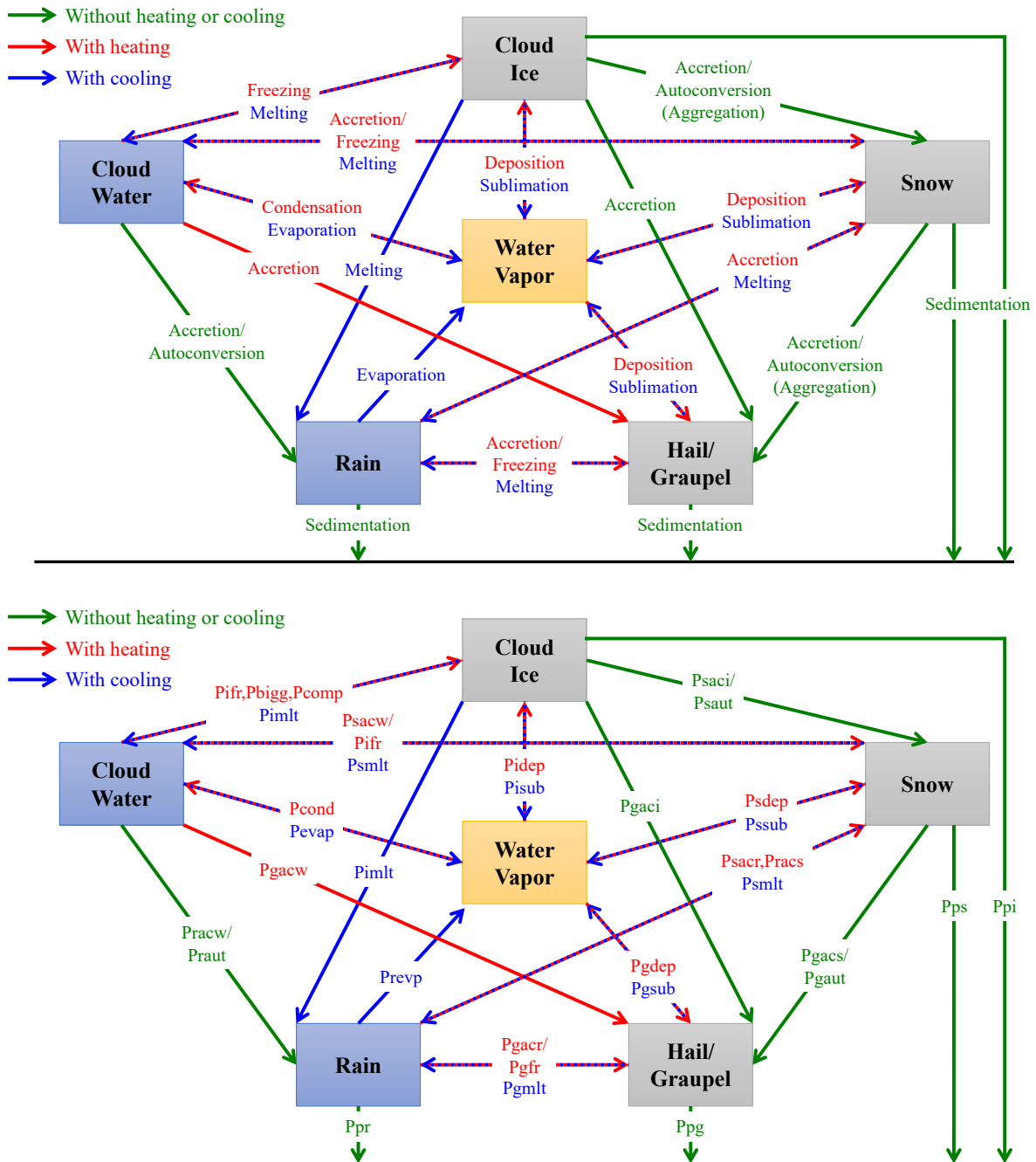
Figure 1: Schematic of the GFDL MP. The yellow box indicates prognostic water vapor, blue boxes indicate prognostic liquid-phase hydrometeors, and gray boxes indicate prognostic solid-phase hydrometeors. Red / Blue arrows indicate processes involving heating / cooling from phase changes, while green arrows indicate conversion and sedimentation processes. The bottom panel shows symbols defined in Table 1 and in Equations (2.1) to (2.6). This figure is revised from Zhou et al. (2019).

Table 1: The symbols used in the prognostic mass mixing ratio equations and Figure 1.

Symbol	Meaning and Source
Pcond	Condensational growth of cloud water (Hong and Lim, 2006).
Pevep	Evaporation of cloud water (Hong and Lim, 2006).
Pifr	Freezing of cloud water to form cloud ice (Lin et al., 1983; Hong and Lim, 2006). Auto-convert to snow if cloud ice exceeds a threshold.
Pbigg	Bigg freezing of cloud water to form cloud ice (Bigg, 1953).
Pcomp	Complete freezing of cloud water to form cloud ice (Lin et al., 1983; Hong and Lim, 2006)
Pidep	Depositional growth of cloud ice (Hong et al., 2004).
Pisub	Sublimation of cloud ice (Hong et al., 2004).
Pimlt	Melting of cloud ice to form cloud water (Lin et al., 1983). Auto-convert to rain if cloud water exceeds a threshold.
Prevp	Evaporation of rain (Lin et al., 1983).
Praut	Auto-conversion of cloud water to form rain (Hong et al., 2004).
Pracw	Accretion of cloud water by rain (Lin et al., 1983).
Pracs	Accretion of snow by rain; produces graupel if rain or snow exceeds a threshold and $T < T_{freez}$ (Lin et al., 1983).
Psacw	Accretion of cloud water by snow; produces snow if $T < T_{freez}$ or rain if $T \geq T_{freez}$ (Lin et al., 1983).
Psacr	Accretion of rain by snow. For $T < T_{freez}$, produces graupel if rain or snow exceeds a threshold; if not, produces snow (Lin et al., 1983).
Psaci	Accretion of cloud ice by snow (Lin et al., 1983).
Psaut	Auto-conversion (aggregation) of cloud ice to form snow (Lin et al., 1983).
Psdep	Depositional growth of snow (Lin et al., 1983).
Pssub	Sublimation of snow (Lin et al., 1983).
Psmlt	Melting of snow to form cloud water (Lin et al., 1983). Auto-convert to rain if cloud water exceeds a threshold.
Pgaut	Auto-conversion (aggregation) of snow to form graupel (Lin et al., 1983).
Pgfr	Freezing of rain to form graupel (Lin et al., 1983).
Pgacw	Accretion of cloud water by graupel (Lin et al., 1983).
Pgaci	Accretion of cloud ice by graupel (Lin et al., 1983).
Pgacr	Accretion of rain by graupel (Lin et al., 1983).
Pgacs	Accretion of snow by graupel (Lin et al., 1983).
Pgdep	Depositional growth of graupel (Lin et al., 1983).
Pgsub	Sublimation of graupel (Lin et al., 1983).
Pgmlt	Melting of graupel to form rain, $T \geq T_{freez}$ (Lin et al., 1983).
Ppi	Sedimentation of cloud ice (Deng and Mace, 2008; Heymsfield and Donner, 1990).
Ppr	Sedimentation of rain (Lin et al., 1983).
Pps	Sedimentation of snow (Lin et al., 1983).
Ppg	Sedimentation of graupel (Lin et al., 1983).

There are several definitions, assumptions, and conservations that are different from other cloud microphysics schemes. The mass of a grid cell includes that of water vapor and of all hydrometeors; that latent heat coefficients are functions of air temperature; dry air, water vapor, liquid water, and solid water have their

own heat capacities; cloud droplet number concentrations are prescribed; subgrid variability is piecewise-linear and scale-aware; saturation water vapor pressure is derived explicitly; latent heating and cooling follow the exact moist total energy conservation. More details will be depicted in this section.

2.2   Vertical Placement of the Meteorological Fields

It is important to clarify in advance where the meteorological fields are located in the model vertical levels / layers. Model levels are defined as the boundaries of the model layers. Thus the number of model levels is equal to one more than the number of model layers. Sometimes, model levels are called as interfaces or layer edges. Meteorological fields at model layers in FV3 are always defined as layer-mean values. However, those at model levels are defined as interface (cell face-mean) values.

As it is shown in Figure 2, interface height (z_{int}) and interface air pressure (p_{int}) are defined at model levels. Zonal wind (u), meridional wind (v), vertical velocity (w), air temperature (T), the mass mixing ratio of hydrometeors (q), height thickness (negative) (dz), pressure thickness or air mass (positive) (dp) are defined at model layers. Those are layer-mean variables. We can also get the middle layer height (z) and layer-mean air pressure (p) using gas law and hydrostatic equilibrium:

$$p = -\frac{dp}{gdz}R_{dry}T_v \tag{2.7}$$

where T_v is virtual temperature, and R_{dry} is dry air constant.
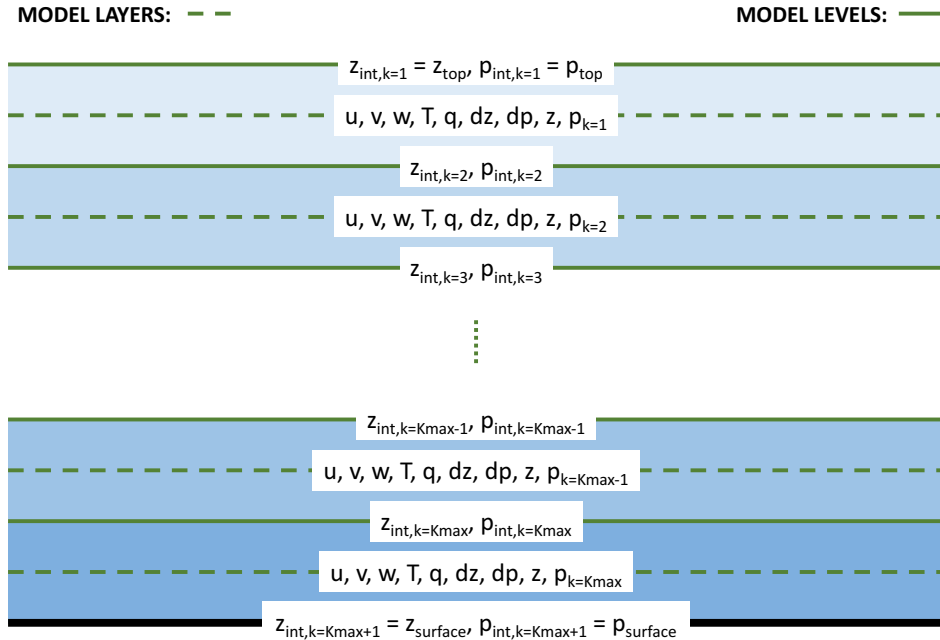
Figure 2: Schematic of model layers, model levels, and the location of different meteorological fields.

2.3 Size Distribution of Hydrometeors

The size distribution of hydrometeors is central to a cloud microphysics scheme (Khain and Pinsky, 2018). Many microphysical variables and processes are directly derived from the integration over the size distribution. For example, the mass mixing ratio of hydrometeors is the third moment. The number concentration of hydrometeor is the zeroth moment, the effective radius is the ratio of the third moment and the second moment, and the radar reflectivity is the sixth moment. The terminal velocity and collision are mostly determined by the higher moments of the size distribution. According to observations, the size distribution of non-precipitable hydrometeors (e.g. cloud water and cloud ice) is represented as a gamma distribution, while precipitable hydrometeors (e.g. rain, snow, and graupel) is represented as a exponential distribution (Pruppacher and Klett, 2010). The exponential distribution can be treated as a simplified gamma distribution.

However, the size distribution of cloud water and cloud ice in the GFDL MP is assumed to be uniform so far, which is simple but unrealistic. Therefore, the number concentration, effective radius, radar reflectivity, and terminal velocity of cloud water and cloud ice are either prescribed as constant or empirically diagnosed from other variables. The size distribution of rain (n_{rain}), snow (n_{snow}), and graupel ($n_{graupel}$) is assumed as an exponential distribution and follows Lin et al. (1983):

$$n_{rain}(D) = n_{rain,0} \exp\left(-\lambda_{rain} D\right) \tag{2.8}$$

$$n_{snow}(D) = n_{snow,0} \exp\left(-\lambda_{snow} D\right) \tag{2.9}$$

$$n_{graupel}(D) = n_{graupel,0} \exp\left(-\lambda_{graupel} D\right) \tag{2.10}$$

where D is the diameter of hydrometeor. $n_{rain,0}$, $n_{snow,0}$, and $n_{graupel,0}$ are the intercept parameters of the rain, snow, and graupel size distributions prescribed as constants. The slope parameters of the rain (λ_{rain}), snow (λ_{snow}), and graupel ($\lambda_{graupel}$) size distributions can be derived from the integration of size distribution for all sizes and the mass mixing ratio of hydrometeor:

$$\lambda_{rain} = \left(\frac{\pi \rho_{rain} n_{rain,0}}{\rho q_{rain}}\right)^{0.25} \tag{2.11}$$

$$\lambda_{snow} = \left(\frac{\pi \rho_{snow} n_{snow,0}}{\rho q_{snow}}\right)^{0.25} \tag{2.12}$$

$$\lambda_{graupel} = \left(\frac{\pi \rho_{graupel} n_{graupel,0}}{\rho q_{graupel}}\right)^{0.25} \tag{2.13}$$

where ρ_{rain}, ρ_{snow}, and $\rho_{graupel}$ are the density of rain, snow, and graupel. ρ is air density.

2.4 Air Mass and Mass Mixing Ratio of Hydrometeors

Air mass per unit area (M_{dry}) and the mass mixing ratio of hydrometeors (q_*) in the GFDL MP are defined for dry air at the model layers:

$$M_{dry} = \frac{dp}{g} \tag{2.14}$$

$$q_* = \frac{M_*}{M_{dry}} \tag{2.15}$$

where dp is dry air thickness, q_* can be q_{vapor}, q_{water}, q_{ice}, q_{rain}, q_{snow}, or $q_{graupel}$, M_* can be M_{vapor}, M_{water}, M_{ice}, M_{rain}, M_{snow}, or $M_{graupel}$. That is different from those in the FV3 dynamical core, which are defined for moist air (dry air + all hydrometeors) thickness (dp') and the specific ratio of hydrometeors (q'_*):

$$dp' = (M_{dry} + M_{vapor} + M_{water} + M_{ice} + M_{rain} + M_{snow} + M_{graupel})\, g \tag{2.16}$$

$$q'_* = \frac{M_*}{M_{dry} + M_{vapor} + M_{water} + M_{ice} + M_{rain} + M_{snow} + M_{graupel}} \tag{2.17}$$

At the beginning of the cloud microphysics scheme, moist air thickness (dp') is converted to dry air thickness (dp), specific ratio of hydrometeors (q'_*) is converted to mass mixing ratio of hydrometeors (q_*):

$$dp = dp' \left[1 - \left(q'_{vapor} + q'_{water} + q'_{ice} + q'_{rain} + q'_{snow} + q'_{graupel}\right)\right] \tag{2.18}$$

$$q_* = \frac{q'_*}{1 - \left(q'_{vapor} + q'_{water} + q'_{ice} + q'_{rain} + q'_{snow} + q'_{graupel}\right)} \tag{2.19}$$

At the end of the cloud microphysics scheme, dry air thickness (dp) converts back to moist air thickness (dp'), mass mixing ratio of hydrometeors (q_*) converts back to specific ratio of hydrometeors (q'_*):

$$dp' = dp \left[1 + (q_{vapor} + q_{water} + q_{ice} + q_{rain} + q_{snow} + q_{graupel})\right] \tag{2.20}$$

$$q'_* = \frac{q_*}{1 + (q_{vapor} + q_{water} + q_{ice} + q_{rain} + q_{snow} + q_{graupel})} \tag{2.21}$$

It is important to note that air mass is exactly conserved in the GFDL MP.

2.5   Number Concentration of Hydrometeors

In the GFDL MP, the number concentration of hydrometeors are not prognostic variables. For cloud water, the number concentration is only used for cloud water to rain autoconversion and cloud water freezing to form cloud ice. It will be described later that the cloud water number concentration is from the prescribed cloud droplet number concentration, which has constant values over land and over ocean. For cloud ice, the number concentration should be from ice nucleation or cloud ice deposition. For now, it follows the calculation in Hong et al. (2004):

$$N_{ice} = 5.38 \times 10^7 \left(\rho q_{ice}\right)^{0.75} \tag{2.22}$$

Optionally, N_{ice} can also be calculated from Meyers et al. (1992):

$$N_{ice} = \exp\left[-2.80 + 0.262 \times (T_{freez} - T)\right] \times 1000.0 \tag{2.23}$$

or

$$N_{ice} = \exp\left[-0.639 + 12.96 \times \left(\frac{q_{vapor}}{q_{s2}} - 1\right)\right] \times 1000.0 \tag{2.24}$$

N_{ice} can also calculated from Cooper (1986):

$$N_{ice} = 5 \times 10^{-3} \times \exp\left[0.304 \times (T_{freez} - T)\right] \times 1000.0 \tag{2.25}$$

One more option is from Fletcher et al. (1962):

$$N_{ice} = 1 \times 10^{-5} \times \exp\left[0.5 \times (T_{freez} - T)\right] \times 1000.0 \tag{2.26}$$

Since rain, snow, and graupel follow the exponential size distribution, Their number concentrations (N_{rain}, N_{snow}, and $N_{graupel}$) are the integration of size distributions:

$$N_{rain} = \int_0^\infty n_{rain}(D)dD = \frac{n_{rain,0}}{\lambda_{rain}} \tag{2.27}$$

$$N_{snow} = \int_0^\infty n_{snow}(D)dD = \frac{n_{snow,0}}{\lambda_{snow}} \tag{2.28}$$

$$N_{graupel} = \int_0^\infty n_{graupel}(D)dD = \frac{n_{graupel,0}}{\lambda_{graupel}} \tag{2.29}$$

If, in the future, number concentration is a prognostic variable in this cloud microphysics scheme, $n_{rain,0}$, $n_{snow,0}$, and $n_{graupel,0}$ will no longer be constants. Instead, they are updated upon the change of mass mixing ratio and number concentration written as:

$$n_{rain,0} = \left(\frac{\pi \rho_{rain}}{\rho q_{rain}}\right)^{1/3} N_{rain}^{4/3} \tag{2.30}$$

$$n_{snow,0} = \left(\frac{\pi \rho_{snow}}{\rho q_{snow}}\right)^{1/3} N_{snow}^{4/3} \tag{2.31}$$

$$n_{graupel,0} = \left(\frac{\pi \rho_{graupel}}{\rho q_{graupel}}\right)^{1/3} N_{graupel}^{4/3} \tag{2.32}$$

2.6   Air Density

Many assumptions in the GFDL MP depend on whether the model, particularly the FV3 dynamical core, is designed to be hydrostatic or non-hydrostatic. For climate modeling, the hydrostatic assumption is appropriate. In this case, the GFDL MP uses the consistent definition of constants and parameters as other physical parameterizations. As the resolutions approach the grey zone, the hydrostatic assumption is no longer as accurate and it is more appropriate to use non-hydrostatic dynamics. In either case, energy conservation and the consistency of constants and parameterizations are critical.

In hydrostatic case, moist air thickness (dp') and air temperature (T) are both prognostic variables in the dynamical core. So air density (ρ) is calculated using the ideal gas law and the hypsometric equation:

$$\rho = \frac{p}{R_{dry}T_v} = \frac{dp'}{d\ln p' R_{dry}T_v} \tag{2.33}$$

where T_v is virtual temperature, R_{dry} is dry air gas constant.

In non-hydrostatic case, the height thickness (negative) (dz) is also a prognostic variable. So air density (ρ) is calculated from its definition:

$$\rho = -\frac{dp'}{gdz} \tag{2.34}$$

where g is gravitational acceleration.

2.7   Virtual Temperature

The virtual temperature (T_v) of a moist air parcel is the temperature at which a theoretical dry air parcel would have a total pressure and density equal to the moist parcel of air. Thus all hydrometeors are considered to calculate virtual temperature:

$$T_v = T\left(1 + z_{vir}q_{vapor}\right)\left[1 - \left(q_{vapor} + q_{water} + q_{ice} + q_{rain} + q_{snow} + q_{graupel}\right)\right]^{\,1} \tag{2.35}$$

where z_{vir} is the ratio of the gas constants of water vapor (R_{vapor}) and dry air (R_{dry}):

$$z_{vir} = \frac{R_{vapor}}{R_{dry}} - 1 \tag{2.36}$$

2.8   Specific Heat Capacity

In the real atmosphere, the air contains water vapor and hydrometeors. Thus, the specific heat capacity consists of contributions from both dry air, water vapor, and each hydrometeor. In the GFDL MP, the constant-volume or constant-pressure specific heat capacity for moist air ($c_{v,moist}$ or $c_{p,moist}$) is defined as:

$$c_{v,moist} = c_{v,dry} + q_{vapor}c_{v,vapor} + q_{liquid}c_{v,liquid} + q_{solid}c_{v,solid} \tag{2.37}$$

$$c_{p,moist} = c_{p,dry} + q_{vapor}c_{p,vapor} + q_{liquid}c_{p,liquid} + q_{solid}c_{p,solid} \tag{2.38}$$

where $c_{v,dry}$, $c_{v,vapor}$, $c_{v,liquid}$, and $c_{v,solid}$ are the constant-volume specific heat capacities of dry air, water vapor, liquid water (at the triple point of water T_{freez}), and solid water (at the triple point of water T_{freez}). Similarly, $c_{p,dry}$, $c_{p,vapor}$, $c_{p,liquid}$, and $c_{p,solid}$ are the corresponding specific heat capacities at constant pressure. Liquid water and solid water barely change in volume and pressure during heating or cooling that their constant-volume and constant-pressure specific heat capacities are the same and defined as:

$$c_{liquid} = c_{v,liquid} = c_{p,liquid} \tag{2.39}$$

$$c_{solid} = c_{v,solid} = c_{p,solid} \tag{2.40}$$

q_{liquid} is the mass mixing ratio of liquid water defined as the sum of the mass mixing ratio of cloud water and rain:

$$q_{liquid} = q_{water} + q_{rain} \tag{2.41}$$

and q_{solid} is the mass mixing ratio of solid water defined as the sum of mass mixing ratio of cloud ice, snow, and graupel:

$$q_{solid} = q_{ice} + q_{snow} + q_{graupel} \tag{2.42}$$

The sum of the mass mixing ratio of liquid and solid water (q_{cond}) is written as:

$$q_{cond} = q_{liquid} + q_{solid} \tag{2.43}$$

---

[1]This differs slightly from the IFS formula: $T_v = T\left[1 + z_{vir}q_{vapor} - \left(q_{vapor} + q_{water} + q_{ice} + q_{rain} + q_{snow} + q_{graupel}\right)\right]$ (https://www.ecmwf.int/en/elibrary/18714-part-iv-physical-processes Chapter 12. The difference is of order $q_{vapor}q_* \ll q_*$ while reducing the number of computations within the code.)

Different from most existing cloud microphysics schemes, the GFDL MP was built at the height coordinate. That means heating or cooling in this cloud microphysics scheme uses the constant-volume specific heat capacity. Pressure thickness is later adjusted according to the change of hydrometeors content in the grid box. This treatment is consistent with what is being used in FV3's nonhydrostatic solver (Lin, 2004), and the Nonhydrostatic ICosahedral Atmospheric Model (NICAM) (Satoh et al., 2008). Theoretically and actually, the constant-pressure specific heat capacity is about 40% larger than the constant-volume specific heat capacity. It indicates the heating or cooling by using constant-pressure specific heat capacity is 40% smaller than that using constant-volume specific heat capacity. Since the height thickness will be later adjusted according to temperature change, the eventual impact of the microphysics processes on the atmosphere is similar in these two different approaches. In the following sections, we use c_{moist} instead of $c_{v,moist}$ as default.

2.9 Latent Heat Coefficient

According to the Kirchhoff's equation under constant volume (Emanuel, 1994), the latent heat coefficient of condensation / evaporation (L_{v2l}), melting / freezing (L_{l2s}), and deposition / sublimation (L_{v2s}) are a function of temperature (T):

$$L_{v2l} = L_{vap} + (c_{vapor} - c_{liquid})(T - T_{freez}) \tag{2.44}$$

$$L_{l2s} = L_{fus} + (c_{liquid} - c_{solid})(T - T_{freez}) \tag{2.45}$$

$$L_{v2s} = L_{vap} + L_{fus} + (c_{vapor} - c_{solid})(T - T_{freez}) \tag{2.46}$$

where L_{vap} and L_{fus} are the latent heat coefficient of condensation / evaporation and melting / freezing at the triple point temperature of water (T_{freez}). $c_{vapor} = c_{p,vapor}$ in hydrostatic case. $c_{vapor} = c_{v,vapor}$ in non-hydrostatic case.

A special latent heat coefficient of condensation / evaporation (L'_{v2l}) for saturated water vapor is defined as:

$$L'_{v2l} = L_{v2l} + L_{l2s} \max \left[0, \min \left(1, \frac{T_{freez} - T}{T_{freez} - T_{wfr}}\right)\right] \tag{2.47}$$

If temperature is higher than freezing temperature ($T > T_{freez}$), $L'_{v2l} = L_{v2l}$; If temperature is lower than critical freezing temperature ($T < T_{wfr}$), $L'_{v2l} = L_{v2s}$; otherwise ($T_{wfr} < T < T_{freez}$), $L_{v2l} < L'_{v2l} < L_{v2s}$.

2.10 Cloud Condensation Nuclei and Cloud Droplet Number Concentration

Cloud condensation nuclei (CCN) is used in cloud seeding, that tries to promote condensation into cloud water by seeding the air with condensation nuclei. It is a major source of cloud water formation. The cloud droplet number concentration (CDNC) activated from CCN determines how much cloud water can be auto-converted to rain. However, since there is no cloud water activation built in this cloud microphysics scheme, the cloud droplet number concentration (CDNC, N_c) is either prescribed over land ($N_{c,land}$) and ocean ($N_{c,ocean}$) respectively:

$$N_c = [N_{c,land} \cdot LSM + N_{c,ocean} \cdot (1 - LSM)] \times 10^6 \tag{2.48}$$

or calculated from aerosol mass mixing ratio ($q_{aerosol}$) following Boucher and Lohmann (1995):

$$N_c = \left[10^{2.24} \times \left(10^9 \rho q_{aerosol}\right)^{0.257} \cdot LSM + 10^{2.06} \times \left(10^9 \rho q_{aerosol}\right)^{0.48} \cdot (1 - LSM)\right] \times 10^6 \tag{2.49}$$

where LSM is the land-sea mask, with value 1 over land and value 0 over ocean. ρ_{bot} is the bottom layer air density. The former method is used in the current operational GFS, NASA GEOS-5, HiRAM, IAP climate model. The latter method is an option in the GFDL modeling system suites. The number concentration of cloud then from the cloud droplet number concentration (CDNC):

$$N_{water} = N_c \tag{2.50}$$

2.11 Subgrid Variability

In a model that is unable to resolve cloud microphysical processes explicitly, it is useful to prescribe the subgrid distribution of quantities (e.g., hydrometeors) in the grid box. Regardless of which algorithm is used, it is some kind of empirical assumption. The simplest one is a linear assumption. In the GFDL MP, it presumed a linear background horizontal variability (h_{var}) and vertical variability (z_{var}) for hydrometeors following Lin et al. (1994).

The horizontal subgrid variability is a function of cell area:

$$h_{var} = \min\left(0.2, \max\left\{0.01, [D_{land} \cdot LSM + D_{ocean} \cdot (1 - LSM)]\sqrt{\frac{x}{10^5}}\right\}\right) \tag{2.51}$$

where x is grid size. D_{land} and D_{ocean} are basic value for subgrid variability over land and ocean. These are tunable parameters. This formula indicates larger subgrid variability appears in the larger cell area. D_{land} and D_{ocean} can adjust the strength of the subgrid variability. The subgrid variability function enables the GFDL MP to be flexibly adapted to simulations in different resolutions and variable resolution. Theoretically, this assumption can be applied to all condensation / evaporation, freezing / melting, and deposition / sublimation processes. In the current version of GFDL MP, horizontal subgrid variability is mainly used in the calculation of cloud water to rain autoconversion and cloud fraction diagnostic.

The vertical subgrid variability depends on the distribution of the three adjacent mass mixing ratio of hydrometeors: for model top ($k = 1$) and bottom layer ($k = kbot$):

$$z_{var,1} = 0 \tag{2.52}$$

$$z_{var,kbot} = 0 \tag{2.53}$$

for all other model layers ($k = 2, kbot - 1$), use twice the strength of the positive definiteness limiter (Lin et al., 1994). Four conditions are considered shown in Figure 3:

1) When $q_{k+1} > q_k$, and $q_k > q_{k-1}$, monotonically increasing from up to down:

$$z_{var,k} = \frac{1}{2}\min\left(\left|\frac{q_{k+1} - q_{k-1}}{2}\right|, \frac{q_k}{2}\right) \tag{2.54}$$

2) When $q_{k+1} < q_k$, and $q_k < q_{k-1}$, monotonically decreasing from up to down:

$$z_{var,k} = \frac{1}{2}\min\left(\left|\frac{q_{k+1} - q_{k-1}}{2}\right|, \frac{q_k}{2}\right) \tag{2.55}$$
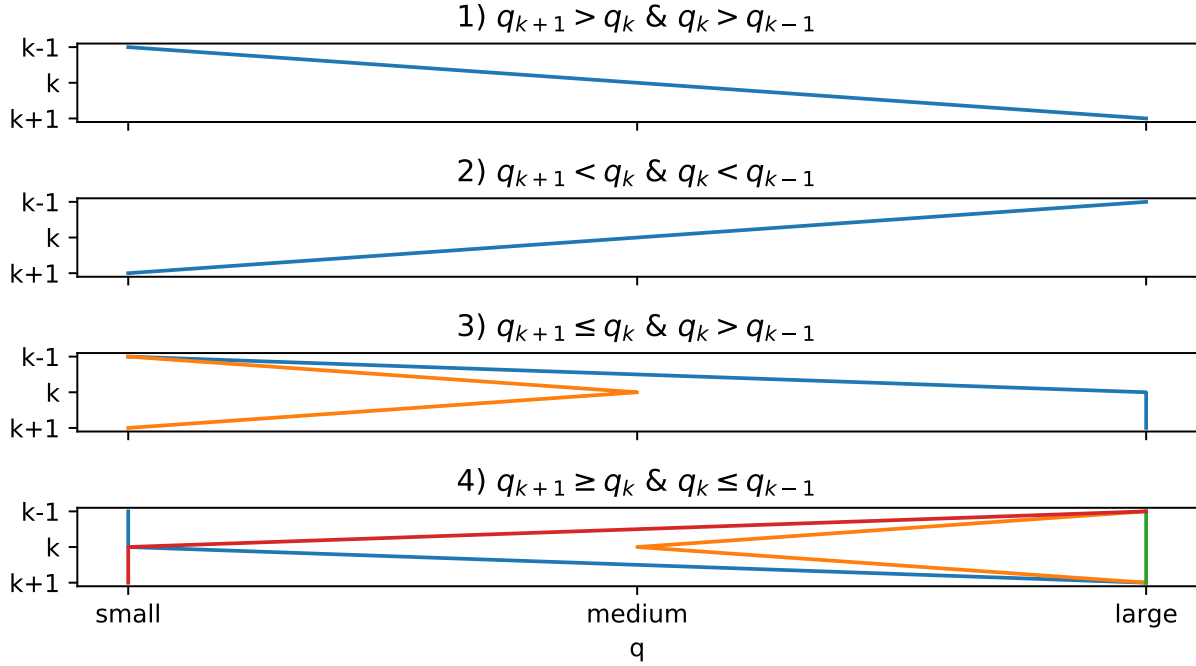
Figure 3: Four different conditions of hydrometeor vertical profile in the adjacent three layers. Blue, orange, and red vertical profiles are three different possibles in each condition.

3) When $q_{k+1} \leq q_k$, and $q_k > q_{k-1}$, maximum value at the center:

$$z_{var,k} = \min \left[\frac{1}{2} \min \left(\left| \frac{q_{k+1} - q_{k-1}}{2} \right|, \frac{q_k}{2} \right), \frac{q_k - q_{k-1}}{2}, -\frac{q_{k+1} - q_k}{2} \right] \tag{2.56}$$

4) When $q_{k+1} \geq q_k$, and $q_k \leq q_{k-1}$, minimum value at the center:

$$z_{var,k} = 0.0 \tag{2.57}$$

Impose a presumed background horizontal variability that is proportional to the value itself:

$$z_{var,k} = \max \left(z_{var,k}, q_{minvapor}, h_{var} q_k \right), \quad k = 1, ..., kbot \tag{2.58}$$

Note that z_{var} is a function of q, so z_{var} is different in each hydrometeor. $q_{minvapor}$ is minimum value for water vapor. Vertical subgrid variability is mainly used in the calculation of cloud water to rain autoconversion.

2.12 Rate of Conversion

In general, conversion between two hydrometeors is not done instantaneously except for some extreme conditions. In most cases, it is a function of time. If the cloud microphysics scheme is embedded in the FV3 dynamical core, it will use the vertical remapping time step (dt_m), which is a sub-cycle of physics time step (dt_p) controlled by *k_split* in the namelists. If the cloud microphysics scheme is inside the normal physics

package, it uses a relative smaller cloud microphysics time step (dt_c), which is also a sub-cycle of physics time step (dt_p). dt_p, dt_m, dt_c at this stage are the same. However, dt_p, dt_m and dt_c have much freedom to control separately, especially for higher resolution.

In many microphysical processes of this cloud microphysics scheme, the effective conversion rate from x to y over a time step dt, assuming an exponential decrease of x, is calculated as:

$$f_{x2y} = 1 - \exp\left(-\frac{dt}{\tau_{x2y}}\right) \tag{2.59}$$

where x and y can be v (water vapor), w (cloud water), i (cloud ice), r (rain), s (snow), or g (graupel). dt can be dt_m or dt_c. Note that τ_{x2y} and α are both tunable parameters controlling the conversion rate. The larger of τ_{x2y}, the slower the conversion.

2.13 Fix Negative Hydrometeors

Unphysical negative hydrometeor concentrations are difficult to completely avoid in finite-precision arithmetic. Fixing negative hydrometeors in the GFDL MP is straightforward and mass conserved. The easiest way to fix negative hydrometeor is to borrow mass from other hydrometeors. Negative hydrometeor then is fixed to zero. Assume hydrometeor x is negative, and borrow mass from hydrometeor y:

$$q_y = q_y + q_x \tag{2.60}$$

$$q_x = 0.0 \tag{2.61}$$

In some certain conditions, q_y could become negative after this process. Then q_y need to be fixed from other hydrometeors except for q_x. In general, the direction of negative fixing follows:

$$q_{ice} \leftarrow q_{snow} \leftarrow q_{graupel} \leftarrow q_{rain} \leftarrow q_{water} \leftarrow q_{vapor} \tag{2.62}$$

That is to say, if q_{ice} is negative, borrow mass from q_{snow}; if q_{snow} is negative, borrow mass from $q_{graupel}$; etc. However, to prevent overdoing, Equation (2.60) can be revised as:

$$q_{tmp} = \min\left[-q_x, \max\left(0, q_y\right)\right] \tag{2.63}$$

$$q_x = q_x + q_{tmp} \tag{2.64}$$

$$q_y = q_y - q_{tmp} \tag{2.65}$$

If this is a phase change, latent heating and cooling should also be applied.

In the GFDL MP, water vapor can be used to fix all other negative hydrometeors. However, when water vapor is negative, it can borrow from above and below layers. From $k = 1$ to $kbot - 1$, when water vapor at k layer is negative, borrow it from below:

$$q_{vapor,k+1} = q_{vapor,k+1} + \frac{q_{vapor,k}dp_k}{dp_{k+1}} \tag{2.66}$$

$$q_{vapor,k} = 0 \tag{2.67}$$

when water vapor at the bottom layer is negative, borrow it from above if the water vapor in $kbot - 1$ is

positive:

$$dq = \min\left[-q_{vapor,kbot}dp_{kbot}, q_{vapor,kbot-1}dp_{kbot-1}\right] \tag{2.68}$$

$$q_{vapor,kbot-1} = q_{vapor,kbot-1} - \frac{dq}{dp_{kbot-1}} \tag{2.69}$$

$$q_{vapor,kbot} = q_{vapor,kbot} + \frac{dq}{dp_{kbot}} \tag{2.70}$$

2.14 Saturation Water Vapor Pressure

Saturation water vapor pressure is calculated using lookup tables. Five lookup tables are designed for different purposes for the GFDL MP. First of all, define a scaled temperature

$$T'^* = \min\left\{2621, 10\left[T - (T_{freez} - 160)\right] + 1\right\} \tag{2.71}$$

$$T^* = \text{INT}\left(T'^*\right) \tag{2.72}$$

INT here means forcing a variable to be an integer. Different from most existing tables of saturation water vapor pressure, which are basically written as empirical formula, the ones in the GFDL MP are directly derived by integrating of the Clausius-Claperyron equation (Wallace and Hobbs, 1977):

$$\frac{d\ln e_{s*}}{dT} = \frac{L_*}{R_{vapor}T^2} \tag{2.73}$$

where e_{s*} can be e_s0, e_{s1}, or e_{s2} detailedly described in the following sub-sections. L_* can be L_{v2l}, L_{l2s}, or L_{v2s}.

Table N

The table N of saturation water vapor pressure (e_{s0}) was built only over water with temperature ranged from $-160°C$ to $102°C$ defined as:

$$T_{tmp} = T_{freez} - 160 + 0.1\left(T^* - 1\right) \tag{2.74}$$

$$\alpha = \frac{(c_{p,vapor} - c_{liquid})\ln\dfrac{T_{tmp}}{T_{freez}} + [L_{vap} - T_{freez}(c_{p,vapor} - c_{liquid})]\dfrac{T_{tmp} - T_{freez}}{T_{tmp}T_{freez}}}{R_{vapor}} \tag{2.75}$$

$$e_{s0}(T^*) = e_0 e^{\alpha} \tag{2.76}$$

Table I

The table I of saturation water vapor pressure (e_{s1}) was built based on three temperature categories:

1) When T^* ranges from 1 to 1600 (T ranges from $-160°C$ to $0°C$), compute saturation water vapor pressure

(e_{s1}) over ice:

$$T_{tmp} = T_{freez} - 160 + 0.1\,(T^* - 1) \tag{2.77}$$

$$\alpha = \frac{(c_{p,vapor} - c_{solid})\ln\dfrac{T_{tmp}}{T_{freez}} + [L_{vap} + L_{fus} - T_{freez}\,(c_{p,vapor} - c_{solid})]\dfrac{T_{tmp} - T_{freez}}{T_{tmp}T_{freez}}}{R_{vapor}} \tag{2.78}$$

$$e_{s1}(T^*) = e_0 e^{\alpha} \tag{2.79}$$

where e_0 is saturation vapor pressure at T_{freez}.

2) When T^* ranges from 1401 to 2621 (T ranges from $-20°C$ to $102°C$), compute saturation water vapor pressure (e_{s1}) over water:

$$T_{tmp} = T_{freez} - 20 + 0.1\,(T^* - 1400 - 1) \tag{2.80}$$

$$\alpha = \frac{(c_{p,vapor} - c_{liquid})\ln\dfrac{T_{tmp}}{T_{freez}} + [L_{vap} - T_{freez}\,(c_{p,vapor} - c_{liquid})]\dfrac{T_{tmp} - T_{freez}}{T_{tmp}T_{freez}}}{R_{vapor}} \tag{2.81}$$

$$e_{s1}(T^*) = e_0 e^{\alpha} \tag{2.82}$$

3) When T^* ranges from 1401 to 1600 (T ranges from $-20°C$ to $0°C$), compute saturation water vapor pressure (e_{s1}) over ice and supercooled water:

$$T_{tmp} = T_{freez} - 20 + 0.1\,(T^* - 1400 - 1) \tag{2.83}$$

$$e_{s1}(T^*) = \frac{(T_{freez} - T_{tmp})}{20}e_{s1}(T^*) + \frac{[T_{tmp} - (T_{freez} - 20)]}{20}e_{s1}(T^*) \tag{2.84}$$

Note that the first $e_{s1}(T^*)$ on the right hand side comes from saturation water vapor pressure over ice between $-160°C$ and $0°C$, and the second $e_{s1}(T^*)$ on the right hand side comes from saturation water vapor pressure over water between $-20°C$ and $102°C$.

Table II

The table II of saturation water vapor pressure (e_{s2}) was built based on two categories:

1) When T^* ranges from 1 to 1600 (T ranges from $-160°C$ to $0°C$), compute saturation water vapor pressure (e_{s2}) over ice:

$$T_{tmp} = T_{freez} - 160 + 0.1\,(T^* - 1) \tag{2.85}$$

$$\alpha = \frac{(c_{p,vapor} - c_{solid})\ln\dfrac{T_{tmp}}{T_{freez}} + [L_{vap} + L_{fus} - T_{freez}\,(c_{p,vapor} - c_{solid})]\dfrac{T_{tmp} - T_{freez}}{T_{tmp}T_{freez}}}{R_{vapor}} \tag{2.86}$$

$$e_{s2}(T^*) = e_0 e^{\alpha} \tag{2.87}$$

2) When T^* ranges from 1601 to 2621 (T ranges from $0°C$ to $102°C$), compute saturation water vapor

pressure (e_{s2}) over water:

$$T_{tmp} = T_{freez} - 160 + 0.1\,(T^* - 1) \tag{2.88}$$

$$\alpha = \frac{(c_{p,vapor} - c_{liquid})\ln\dfrac{T_{tmp}}{T_{freez}} + [L_{vap} - T_{freez}\,(c_{p,vapor} - c_{liquid})]\dfrac{T_{tmp} - T_{freez}}{T_{tmp}T_{freez}}}{R_{vapor}} \tag{2.89}$$

$$e_{s2}(T^*) = e_0 e^{\alpha} \tag{2.90}$$

A smoother was added to e_{s2} where temperature is around $0°C$ ($T^* = 1600$ and $T^* = 1601$):

$$e_{s2}(T^*) = 0.25 e_{s2}(T^* - 1) + 2e_s(T^*) + e_{s2}(T^* + 1) \tag{2.91}$$

Table III

The table III of saturation water vapor pressure (e_{s3}) is the same as Table I except using the Smithsonian formula Smithsonian and List (1951):

1) When T^* ranges from 1 to 1600 (T ranges from $-160°C$ to $0°C$), compute saturation water vapor pressure (e_{s3}) over ice:

$$T_{tmp} = T_{freez} - 160 + 0.1\,(T^* - 1) \tag{2.92}$$

$$a = -9.09718 \times \left(\frac{T_{freez}}{T_{tmp}} - 1\right) \tag{2.93}$$

$$b = -3.56654 \times \log_{10}\left(\frac{T_{freez}}{T_{tmp}}\right) \tag{2.94}$$

$$c = -0.876793 \times \left(\frac{T_{tmp}}{T_{freez}} - 1\right) \tag{2.95}$$

$$e = \log_{10}(6107.1) \tag{2.96}$$

$$e_{s3}(T^*) = 0.1 \times 10^{a+b+c+d} \tag{2.97}$$

2) When T^* ranges from 1401 to 2621 (T ranges from $-20°C$ to $102°C$), compute saturation water vapor

pressure (e_{s3}) over water:

$$T_{tmp} = T_{freez} - 20 + 0.1\,(T^* - 1400 - 1) \tag{2.98}$$

$$a = -7.90298 \times \left(\frac{T_{freez} + 100}{T_{tmp}} - 1.\right) \tag{2.99}$$

$$b = 5.02808 \times \log_{10}\left(\frac{T_{freez} + 100}{T_{tmp}}\right) \tag{2.100}$$

$$c = -1.3816 \times 10^{-7} \times \left[10^{11.344 \times \left(1 - \frac{T_{tmp}}{T_{freez} + 100}\right)} - 1\right] \tag{2.101}$$

$$d = 8.1328 \times 10^{-3} \times \left[10^{3.49149 \times \left(1 - \frac{T_{freez} + 100}{T_{tmp}}\right)} - 1.\right] \tag{2.102}$$

$$e = \log_{10}(1013246.0) \tag{2.103}$$

$$e_{s3}(T^*) = 0.1 \times 10^{a+b+c+d} \tag{2.104}$$

3) When T^* ranges from 1401 to 1600 (T ranges from $-20°C$ to $0°C$), compute saturation water vapor pressure (e_{s3}) over ice and supercooled water:

$$T_{tmp} = T_{freez} - 20 + 0.1\,(T^* - 1400 - 1) \tag{2.105}$$

$$e_{s3}(T^*) = \frac{(T_{freez} - T_{tmp})}{20} e_{s3}(T^*) + \frac{[T_{tmp} - (T_{freez} - 20)]}{20} e_{s3}(T^*) \tag{2.106}$$

Note that the first $e_{s3}(T^*)$ on the right hand side comes from saturation water vapor pressure over ice between $-160°C$ and $0°C$, and the second $e_{s3}(T^*)$ on the right hand side comes from saturation water vapor pressure over water between $-20°C$ and $102°C$.

Table IV

The table IV of saturation water vapor pressure (e_{s4}) is the same as Table II except using the Smithsonian formula Smithsonian and List (1951):

1) When T^* ranges from 1 to 1600 (T ranges from $-160°C$ to $0°C$), compute saturation water vapor pressure (e_{s4}) over ice:

$$T_{tmp} = T_{freez} - 160 + 0.1\,(T^* - 1) \tag{2.107}$$

$$a = -9.09718 \times \left(\frac{T_{freez}}{T_{tmp}} - 1\right) \tag{2.108}$$

$$b = -3.56654 \times \log_{10}\left(\frac{T_{freez}}{T_{tmp}}\right) \tag{2.109}$$

$$c = -0.876793 \times \left(\frac{T_{tmp}}{T_{freez}} - 1\right) \tag{2.110}$$

$$e = \log_{10}(6107.1) \tag{2.111}$$

$$e_{s3}(T^*) = 0.1 \times 10^{a+b+c+d} \tag{2.112}$$

2) When T^* ranges from 1601 to 2621 (T ranges from $0°C$ to $102°C$), compute saturation water vapor pressure (e_{s4}) over water:

$$T_{tmp} = T_{freez} - 20 + 0.1 \left(T^* - 1400 - 1 \right) \tag{2.113}$$

$$a = -7.90298 \times \left(\frac{T_{freez} + 100}{T_{tmp}} - 1. \right) \tag{2.114}$$

$$b = 5.02808 \times \log_{10} \left(\frac{T_{freez} + 100}{T_{tmp}} \right) \tag{2.115}$$

$$c = -1.3816 \times 10^{-7} \times \left[10^{11.344 \times \left(1 - \frac{T_{tmp}}{T_{freez} + 100} \right)} - 1 \right] \tag{2.116}$$

$$d = 8.1328 \times 10^{-3} \times \left[10^{3.49149 \times \left(1 - \frac{T_{freez} + 100}{T_{tmp}} \right)} - 1. \right] \tag{2.117}$$

$$e = \log_{10} \left(1013246.0 \right) \tag{2.118}$$

$$e_{s3}(T^*) = 0.1 \times 10^{a+b+c+d} \tag{2.119}$$

A smoother was added to e_{s4} where temperature is around $0°C$ ($T^* = 1600$ and $T^* = 1601$):

$$e_{s4}(T^*) = 0.25 e_{s4}(T^* - 1) + 2 e_s(T^*) + e_{s4}(T^* + 1) \tag{2.120}$$

Finally

The increment of saturation water vapor pressure is defined as:

$$de_s(T^*) = \max \left[0, e_s(T^* + 1) - e_s(T^*) \right] \tag{2.121}$$

Then the saturated specific humidity is calculated as:

$$q_s(T) = \frac{\rho_s}{\rho} = \frac{\frac{e_s}{R_{vapor} T}}{\rho} = \frac{e_s(T^*) + \left[T'^* - T^* \right] de_s(T^*)}{\rho R_{vapor} T} \tag{2.122}$$

Then the gradient of saturated specific humidity is calculated as:

$$T_{tmp}^* = \text{INT} \left(T'^* - 0.5 \right) \tag{2.123}$$

$$\frac{1}{\rho R_{vapor} T} \frac{de_s(T)}{dT} = \frac{e_s(T + 0.1) - e_s(T)}{0.1 \rho R_{vapor} T} = 10 \frac{de_s(T_{tmp}^*) + \left(T'^* - T_{tmp}^* \right) \left[de_s(T_{tmp}^* + 1) - de_s(T_{tmp}^*) \right]}{\rho R_{vapor} T} \tag{2.124}$$

Here we use finite temperature difference: $dT = 0.1$.

2.15 Energy Conservation

The total energy is precisely conserved all the time in the GFDL MP. Total energy consists of internal energy, potential energy, and kinetic energy. For cloud microphysics processes except for sedimentation, the internal

energy is the only one need to be conserved during phase change. Internal energy (IE) is defined following Emanuel (1994) using the moist specific heat capacity:

$$IE = c_{moist}T + L_v q_{vapor} - L_f \left(q_{ice} + q_{snow} + q_{graupel} \right) \tag{2.125}$$

where $L_v = L_{vap} - (c_{v,vapor} - c_{v,liquid}) T_{freez}$ is a constant latent heat coefficient for condensation / evaporation at $0\ K$, $L_f = L_{fus} - (c_{v,liquid} - c_{v,solid}) T_{freez}$ is a constant latent heat coefficient for freezing / melting at $0\ K$. We can derive the temperature change (ΔT) for condensation / evaporation, freezing / melting, and deposition / sublimation with Δq as

$$\Delta T = \begin{cases} \dfrac{L_{v2l}^n}{c_{moist}^{n+1}} \cdot \Delta q, & \text{condensation / evaporation} \\[2ex] \dfrac{L_{l2s}^n}{c_{moist}^{n+1}} \cdot \Delta q, & \text{freezing / melting} \\[2ex] \dfrac{L_{v2s}^n}{c_{moist}^{n+1}} \cdot \Delta q, & \text{deposition / sublimation} \end{cases} \tag{2.126}$$

where $\Delta T = T^{n+1} - T^n$, and $\Delta q = q^{n+1} - q^n$. n and $n+1$ denote the states before and after the microphysical process. The traditional method to calculate heating in most cloud microphysics schemes is using the constant-pressure specific heat for dry air and latent heat coefficient at T_{freez}.

3 Cloud Microphysical Processes

Many cloud microphysical processes parameterized in this scheme as shown in Figure 1. They can be categorized as the following groups:

- Phase change involved water vapor, e.g., condensation and evaporation, deposition and sublimation;
- Phase change between liquid water and solid water, e.g., freezing and melting;
- Phase change within the same water phase, e.g., autoconversion or aggregation;
- Accretion or collision between two different categories.

3.1 Cloud Water Condensation and Evaporation

When water vapor is saturated, water vapor condenses to cloud water. When water vapor is undersaturated, cloud water evaporates to water vapor. The algorithms of these conversions follow Equation (A46) in Hong and Lim (2006), which followed Yau and Austin (1979), but revised using temperature gradient of saturated specific humidity followed Clausius-Clapeyron equation:

$$\frac{d \ln e_{s*}}{dT} = \frac{L_*}{R_{vapor} T^2} \tag{3.1}$$

or

$$\frac{1}{e_{s*}} \frac{de_{s*}}{dT} = \frac{1}{q_{s*} \rho R_v T} \frac{de_{s*}}{dT} = \frac{L_*}{R_{vapor} T^2} \rightarrow \frac{1}{\rho R_v T} \frac{de_{s*}}{dT} = \frac{L_* q_{s*}}{R_{vapor} T^2} \tag{3.2}$$

where q_{s*} can be q_{s0}, q_{s1}, or q_{s2}. L_* can be L_{v2l} or L'_{v2l}, So the amount of condensation / evaporation per time step can be written as:

$$Pcond' = \frac{q_{vapor} - q_{s0}}{\left(1 + \dfrac{L'_{v2l}}{c_{moist}} \dfrac{1}{\rho R_v T} \dfrac{de_{s0}}{dT}\right) dt}, \quad q_{vapor} > q_{s0} \tag{3.3}$$

$$Pevap' = -\frac{q_{vapor} - q_{s0}}{\left(1 + \dfrac{L'_{v2l}}{c_{moist}} \dfrac{1}{\rho R_v T} \dfrac{de_{s0}}{dT}\right) dt}, \quad q_{vapor} \leq q_{s0} \tag{3.4}$$

1) If water vapor is under-saturated ($q_{vapor} \leq q_{s0}$), cloud water will evaporate to water vapor using f_{w2v} and relative humidity ($RH = q_{vapor}/q_{s0}$) as scaling factors. So the amount of cloud water evaporated to water vapor per time step can be written as:

$$Pevap = \min\left[\frac{q_{water}}{dt}, \min\left(1, f_{w2v} \frac{1 - RH}{1.0 - 0.9}\right) Pevap'\right] \tag{3.5}$$

It is designed for that when relative humidity is low, it would be easier to evaporate, while relative humidity is high, it would be harder to evaporate.

2) If water vapor is saturated ($q_{vapor} > q_{s0}$), use f_{v2w} and relative humidity ($RH = q_{vapor}/q_{s0}$) to prevent over-condensation. So the amount of water vapor condensed to cloud water per time step can be written as:

$$Pcond = \min\left[\frac{q_{vapor}}{dt}, \min\left(1, f_{v2w} \frac{RH - 1}{1.0 - 0.9}\right) Pcond'\right] \tag{3.6}$$

3) If no condensation time scale is predefined, the amount of water vapor condensed to cloud water per time step can be simplified as:

$$Pcond = \min\left[\frac{q_{vapor}}{dt}, Pcond'\right] \tag{3.7}$$

3.2   Evaporation of Rain to Water Vapor

When rain exists at where temperature (T) is higher than T_{wfr}. The evaporation of rain follows the Equation (52) in Lin et al. (1983), but with substantial revision. Firstly, the presence of clouds suppresses the rain evaporation. So define a 'liquid-frozen water temperature' assuming all cloud water have been evaporated:

$$T_{in} = \frac{c_{moist}T - L_v q_{water}}{c_{v,dry} + (q_{vapor} + q_{water})\,c_{v,vapor} + q_{rain}c_{liquid} + (q_{ice} + q_{snow} + q_{graupel})\,c_{solid}} \tag{3.8}$$

Hence the whole rain evaporation process is using T_{in} instead of T. Consistently, assume that all cloud water has been evaporated to water vapor. Secondly, subgrid variability is applied here. Subgrid variability defines an upper bound (q_{plus}) and a lower bound (q_{minus}). Calculation of upper bound and lower bound is based on the linear theory (Lin et al., 1994). The dispersion of $q_{vapor} + q_{water}$ is controlled by the horizontal subgrid variability h_{var} and constrained by cloud water amount. Meanwhile, the dispersion should not exceed its 20%:

$$q_h = \min\left\{\max\left[q_{water}, h_{var}\max\left(q_{vapor} + q_{water}, q_{mincond}\right)\right], 0.2\left(q_{vapor} + q_{water}\right)\right\} \tag{3.9}$$

where $q_{mincond}$ is the minimum value for cloud condensates. Therefore, the upper bound and lower bound are defined as:

$$q_{plus} = q_{vapor} + q_{water} + q_h \tag{3.10}$$

$$q_{minus} = q_{vapor} + q_{water} - q_h \tag{3.11}$$

Rain evaporation starts when water vapor is undersaturated $(q_{vapor} + q_{minvapor} < q_{s0})$ and $q_{minus} < q_{s0}$. The supersaturation of $q_{vapor} + q_{water}$ is defined as:

$$dq = \begin{cases} q_{s0} - (q_{vapor} + q_{water}), & \text{if } q_{plus} < q_{s0} \\ 0.25\dfrac{(q_{s0} - q_{minus})^2}{q_h}, & \text{if } q_{minus} < q_{s0} \leq q_{plus} \end{cases} \tag{3.12}$$

Here q_{s0} is calculated based on T_{in}. According to this formula, if $q_{s0} = q_{minus}$, $dq = 0$; if $q_{s0} = q_{vapor} + q_{water}$, $dq = 0.25q_h$; if $q_{s0} = q_{plus}$, $dq = q_h$.

The amount of rain evaporated to water vapor per time step following Equation (52) in Lin et al. (1983):

$$C = \frac{\rho L_{vap}^2}{K_a R_{vapor} T_{in}^2} \tag{3.13}$$

$$D = \frac{1}{q_{s0}\chi} \tag{3.14}$$

$$Prevp' = \frac{2\pi dq}{q_{s0}\,(C+D)}n_{rain,0}\left[0.78\lambda_{rain}^{-2} + 0.31S_c^{1/3}\Gamma\left(\frac{b+5}{2}\right)a^{1/2}\left(\frac{\rho_{sfc}}{\rho}\right)^{1/4}\nu^{-1/2}\lambda_{rain}^{-(b+5)/2}\right] \tag{3.15}$$

where a and b are constant in empirical formula for U_R defined in Lin et al. (1983).

Meanwhile, rain evaporation can be achieved through saturation adjustment. The amount of rain evaporated to water vapor per time step can be written as:

$$Prevp'' = -\frac{q_{vapor} - q_{s0}}{\left(1 + \frac{L_{v2l}}{c_{moist}} \frac{1}{\rho R_v T} \frac{de_{s0}}{dT}\right) dt} \tag{3.16}$$

Evaporation will stop when all rain is evaporated, or the water vapor is saturated. So the amount of rain evaporated to water vapor per time step can be rewritten as

$$Prevp = \min\left[\frac{q_{rain}}{dt}, f_{r2v}Prevp', Prevp''\right] \tag{3.17}$$

Note that rain evaporation is scaled by the relaxation time f_{r2v}. There is an optional threshold (RH_{revap}) that above of which the rain evaporation is shut off.

3.3 Minimum Evaporation of Rain to Water Vapor

In GFDL MP, there is an option to turn on alternative minimum evaporation in the dry environmental air. Define the relative humidity for rain

$$RH_{rain} = \max\left(0.35, RH_{adj} - RH_{inr}\right) \tag{3.18}$$

Here 0.35 is a lower bound of relative humidity for rain, smaller value makes the rain evaporation harder, vice verses. RH_{inr} is relative humidity increment for minimum evaporation of rain. Evaporation will stop when all rain is evaporated, or the water vapor reaches the rain evaporation saturation. So the amount of rain evaporated to water vapor per time step can be written as:

$$Prevp = \min\left[\frac{q_{rain}}{dt}, -\frac{\min\left(q_{vapor} - RH_{rain}q_{s0}, 0\right)}{\left(1 + \frac{L_{v2l}}{c_{moist}} \frac{1}{\rho R_v T} \frac{de_{s0}}{dT}\right) dt}\right] \tag{3.19}$$

3.4 Cloud Ice Sublimation and Deposition

Cloud ice sublimation or deposition starts only when air temperature (T) is lower than freezing temperature (T_{freez}). To mimic cloud ice nucleation, cloud ice deposition ($Pidep'$) starts when cloud ice exists. $Pidep'$ is defined using Equation (9) in Hong et al. (2004), its A and B are defined in Equation (B8) in Dudhia (1989), and Equation (A15) in Rutledge and Hobbs (1984). The amount of water vapor deposited to cloud ice per time step can be written as:

$$A = \frac{\rho\left(L_{vap} + L_{fus}\right)^2}{K_a R_{vapor} T^2} \tag{3.20}$$

$$B = \frac{1}{q_{s2}\chi} \tag{3.21}$$

$$Pidep' = \frac{4\bar{D}_{conice}\left(q_{vapor} - q_{s2}\right)\left(\rho q_{ice} N_{ice}\right)^{0.5}}{q_{s2}\left(A + B\right)} \tag{3.22}$$

where $\bar{D}_{conice}$ uses the same as Equation (5b) in Hong et al. (2004), N_{ice} is the number concentration of cloud ice, K_a is thermal conductivity of air. χ is diffusivity of water vapor in the air. N_{ice} has the option to get the value from N_i, which comes from cloud ice activation or nucleation.

Meanwhile, cloud ice sublimation or deposition can be achieved through saturation adjustment. The amount of water vapor deposited to cloud ice per time step can be written as:

$$Pidep'' = \frac{q_{vapor} - q_{s2}}{\left(1 + \dfrac{L_{v2s}}{c_{moist}} \dfrac{1}{\rho R_v T} \dfrac{de_{s2}}{dT}\right) dt} \tag{3.23}$$

1) If water vapor is saturated ($q_{vapor} > q_{s2}$), water vapor deposits to cloud ice until temperature reaches freezing temperature T_{freez}. So the amount of water vapor deposited to cloud ice per time step can be written as:

$$Pidep = \min\left[Pidep'', \max\left(\frac{q_{crtice} - q_{ice}}{dt}, Pidep'\right), -\frac{c_{moist}}{L_{v2s}}\frac{T - T_{freez}}{dt}\right] \tag{3.24}$$

where q_{crtice} is initial ice nuclei mass mixing ratio revised from q_{I0} in Equation (7) in Hong et al. (2004):

$$q_{crtice} = \frac{q_{genice}}{\rho} \min\left(q_{limice}, -\frac{T - T_{freez}}{10}\right) \tag{3.25}$$

where q_{genice} is maximum cloud ice generated during remapping time step. q_{limice} is a cloud ice limiter to prevent large ice build-up.

2) If water vapor is under saturated ($q_{vapor} \leq q_{s2}$), cloud ice sublimates to water vapor until temperature (T) reaches the super low temperature (T_{sub}) or all cloud ice is sublimated. So the amount of cloud ice sublimated to water vapor per time step can be written as:

$$Pisub = \min\left\{\frac{q_{ice}}{dt}, -Pidep'', -\min\left[1, \frac{\max(T - T_{sub}, 0)}{5}\right] Pidep'\right\} \tag{3.26}$$

3.5   Snow Sublimation and Deposition

Snow sublimation or deposition starts only when air temperature (T) is lower than freezing temperature (T_{freez}). To mimic cloud ice nucleation, snow deposition ($Psdep'$) starts when snow exists. $Psdep'$ is defined using Equation (31) in Lin et al. (1983). The amount of water vapor deposited to snow per time step can be written as:

$$Psdep' = \frac{2\pi (q_{varpor} - q_{s2})}{q_{s2}(A + B)} n_{snow,0} \left[0.78\lambda_{snow}^{-2} + 0.31 S_c^{1/3}\Gamma\left(\frac{d + 5}{2}\right) c^{1/2}\left(\frac{\rho_{sfc}}{\rho}\right)^{1/4} \nu^{-1/2}\lambda_{snow}^{-(d+5)/2}\right] \tag{3.27}$$

where S_c is Schmidt number. c and d are constant in empirical formula for U_S defined in Lin et al. (1983). ν is kinematic viscosity of air.

Meanwhile, snow sublimation or deposition can be achieved through saturation adjustment. The amount of water vapor deposited to snow per time step can be written as:

$$Psdep'' = \frac{q_{vapor} - q_{s2}}{\left(1 + \dfrac{L_{v2s}}{c_{moist}} \dfrac{1}{\rho R_v T} \dfrac{de_{s2}}{dT}\right) dt} \tag{3.28}$$

1) If water vapor is saturated ($q_{vapor} > q_{s2}$), water vapor deposits to snow until temperature freezing temperature T_{freez}. So the amount of water vapor deposited to snow per time step can be written as:

$$Psdep = \min\left[Psdep'', Psdep', -\frac{c_{moist}}{L_{v2s}}\frac{T - T_{freez}}{dt}\right] \tag{3.29}$$

2) If water vapor is under saturated ($q_{vapor} \leq q_{s2}$), snow sublimates to water vapor until temperature (T) reaches the super low temperature (T_{sub}) or all snow is sublimated. So the amount of snow sublimated to water vapor per time step can be written as:

$$Pssub = \min\left[\frac{q_{snow}}{dt}, -\min\left(1, \frac{T - T_{sub}}{5}\right)Psdep'\right] \tag{3.30}$$

3.6   Graupel Sublimation and Deposition

Graupel sublimation or deposition starts only when air temperature (T) is lower than freezing temperature (T_{freez}). To mimic cloud ice nucleation, graupel deposition ($Pgdep'$) starts when graupel exists. $Pgdep'$ is defined using Equation (46) in Lin et al. (1983). The amount of water vapor deposited to graupel per time step can be written as:

$$Pgdep' = \frac{2\pi\left(q_{varpor} - q_{s2}\right)}{q_{s2}\left(A + B\right)}n_{graupel,0}\left[0.78\lambda_{greupel}^{-2} + 0.31S_c^{1/3}\Gamma\left(\frac{f+5}{2}\right)e^{1/2}\left(\frac{4g\rho_{graupel}}{3C_D\rho}\right)^{1/4}\nu^{-1/2}\lambda_{graupel}^{-(f+5)/2}\right] \tag{3.31}$$

where C_D follows Equation (46) in Lin et al. (1983) defined as:

$$C_D = \frac{4g\rho_{graupel}}{3\rho_{sfc}40.74^2} \tag{3.32}$$

Meanwhile, graupel sublimation or deposition can be achieved through saturation adjustment. The amount of water vapor deposited to graupel per time step can be written as:

$$Pgdep'' = \frac{q_{vapor} - q_{s2}}{\left(1 + \dfrac{L_{v2s}}{c_{moist}}\dfrac{1}{\rho R_v T}\dfrac{de_{s2}}{dT}\right)dt} \tag{3.33}$$

1) If water vapor is saturated ($q_{vapor} > q_{s2}$), water vapor deposits to graupel until temperature freezing temperature T_{freez}. So the amount of water vapor deposited to graupel per time step can be written as:

$$Pgdep = \min\left[Pgdep'', Pgdep', -\frac{c_{moist}}{L_{v2s}}\frac{T - T_{freez}}{dt}\right] \tag{3.34}$$

2) If water vapor is under saturated ($q_{vapor} \leq q_{s2}$), graupel sublimates to water vapor until temperature (T) reaches the super low temperature (T_{sub}) or all graupel is sublimated. So the amount of snow sublimated to water vapor per time step can be written as:

$$Pgsub = \min\left[\frac{q_{graupel}}{dt}, -\min\left(1, \frac{T - T_{sub}}{5}\right)Pgdep'\right] \tag{3.35}$$

3.7 Instantaneous Deposition of Water Vapor

If the air temperature (T) is super low $(T < T_{sub})$, where T_{sub} is the minimum temperature for the sublimation of cloud ice, freeze water vapor as a fix because it is too cold to be accurate. So the amount of water vapor deposited to cloud ice per time step can be written as:

$$Pidep = \frac{q_{vapor} - q_{mincond}}{dt} \tag{3.36}$$

3.8 Instantaneous Evaporation / Sublimation of Cloud Water / Cloud Ice

If the relative humidity is lower than a certain threshold (RH_{adj}), all clouds should evaporate or sublimate to water vapor, results in cloud-free. Assume all cloud water is evaporated to water vapor, all cloud ice is sublimated to water vapor, a new air temperature named 'liquid-frozen water temperature' (T_{in}) is defined:

$$T_{in} = \frac{c_{moist}T - L_f q_{ice} - L_v \left(q_{water} + q_{ice}\right)}{c_{v,dry} + \left(q_{vapor} + q_{water} + q_{ice}\right)c_{v,vapor} + q_{rain}c_{liquid} + \left(q_{snow} + q_{graupel}\right)c_{solid}} \tag{3.37}$$

T_{in} then is used to calculate saturated water vapor pressure q_{s2}. Define relative humidity considering water vapor, cloud water, and cloud ice assumed all cloud water evaporates and all cloud ice sublimates:

$$RH = \frac{q_{vapor} + q_{water} + q_{ice}}{q_{s2}} \tag{3.38}$$

Instant evaporation / sublimation happens when temperature T_{in} is higher than $T_{sub} + 6$, and relative humidity RH is lower than RH_{adj}. So the amount of cloud water / cloud ice evaporated / sublimated to water vapor per time step can be written as:

$$Pevap = \frac{q_{water}}{dt} \tag{3.39}$$

$$Pisub = \frac{q_{ice}}{dt} \tag{3.40}$$

Here the definition of RH_{adj} using horizontal subgrid variability:

$$RH_{adj} = 1 - h_{var} - RH_{inc} \tag{3.41}$$

where RH_{inc} is relative humidity increment for complete evaporation / sublimation of cloud water / cloud ice.

3.9 Melting of Cloud Ice to Cloud Water and Rain

When cloud ice exists at where temperature (T) is higher than freezing temperature (T_{freez}), cloud ice melts to cloud water or rain. The amount of cloud ice melted per time step can be written as:

$$Pimlt' = f_{i2w}\frac{c_{moist}}{L_{l2s}}\frac{T - T_{freez}}{dt} \tag{3.42}$$

Note that the melting process is scaled by a relaxation time f_{i2w}. Melting stops when temperature reaches the freezing temperature or all cloud ice is melted:

$$Pimlt = \min\left(\frac{q_{ice}}{dt}, Pimlt'\right) \tag{3.43}$$

Define $q_{mltwater}$, maximum value of cloud water allowed from melted cloud ice, exceed of which is converted to rain. It is used to prevent excessive cloud water. So the ratio of converted cloud water and total melted cloud ice (α) can be written as:

$$\alpha = \min\left[1, \frac{\max\left(q_{mltwater} - q_{water}, 0\right)}{Pimlt \cdot dt}\right] \tag{3.44}$$

Thus, the ratio of converted rain and total melted cloud ice is $1 - \alpha$.

3.10   Complete Freezing of Cloud Water to Cloud Ice

When temperature (T) is below a critical temperature (T_{wfr}), all cloud water is enforced to freeze to cloud ice. The amount of cloud water frozen to cloud ice per time step can be written as:

$$Pcomp' = -\frac{T - T_{wfr}}{dt_{fr}}\frac{q_{water}}{dt} \tag{3.45}$$

Freezing stops when temperature reaches the critical temperature or all cloud water is frozen:

$$Pcomp = \min\left(\frac{q_{water}}{dt}, Pcomp', -\frac{c_{moist}}{L_{l2s}}\frac{T - T_{wfr}}{dt}\right) \tag{3.46}$$

3.11   Homogeneous Freezing of Cloud Water to Cloud Ice and Snow

Homogeneous freezing is the process by which a supercooled liquid drop freezes without the assistance of ice nuclei. Homogeneous freezing starts when the temperature (T) is lower than T_{wfr}. Cloud water below $T_{wfr} - dt_{fr}$ would be enforced to convert to cloud ice completely. Between $T_{wfr} - dt_{fr}$ and T_{wfr}, the conversion rate is a linear function of temperature. The amount of frozen cloud water per time step can be written as:

$$Pifr' = -\frac{T - T_{wfr}}{dt_{fr}}\frac{q_{water}}{dt} \tag{3.47}$$

The freezing process stops when the temperature reaches T_{wfr} or all cloud water is frozen:

$$Pifr = \min\left(\frac{q_{water}}{dt}, Pifr', -\frac{c_{moist}}{L_{l2s}}\frac{T - T_{wfr}}{dt}\right) \tag{3.48}$$

At this point, $Pift = Pcomp$. However, homogeneous freezing allows exceeded cloud ice to autoconvert to snow. The ratio of converted cloud ice to total frozen cloud water (β) can be written as:

$$\beta = \min\left[1, \frac{\max\left(\frac{q_{autice}}{\rho} - q_{ice}, 0\right)}{Pifr \cdot dt}\right] \tag{3.49}$$

Thus, the ratio of converted snow and total frozen cloud water is $1 - \beta$.

3.12   Bigg Freezing of Cloud Water to Cloud Ice

Different from complete or homogeneous freezing above, Bigg (1953) confirmed that there was a linear relationship between the logarithm of the cloud water diameter and the mean freezing temperature and interpreting his results in terms of simple probability theory. Bigg (1953) can be treated as heterogeneous freezing. Heterogeneous freezing is the process by which a supercooled liquid drop freezes with the assistance of a solid aerosol particle which can act as ice nuclei. The constants are similar to Equation (A.22) in Reisner et al. (1998) or Equation (A44) in Hong and Lim (2006). When cloud water exists at where temperature (T) is lower than freezing temperature (T_{freez}). The amount of cloud water frozen to cloud ice per time step can be written as:

$$Pbigg' = B' \left\{ \exp \left[-A' \left(T - T_{freez} \right) - 1 \right] \right\} \frac{\rho q_{water}^2}{\rho_{water} N_{water}} \tag{3.50}$$

where A' and B' are tunable parameters, ρ_{water} is the density of cloud water, N_{water} is the number concentration of cloud water. The number concentration of cloud water (N_{water}) is from the cloud droplet number concentration (N_c). The freezing process stops when the temperature reaches freezing temperature, or all cloud water is frozen:

$$Pbigg = \min \left(\frac{q_{water}}{dt}, Pbigg', -\frac{c_{moist}}{L_{l2i}} \frac{T - T_{freez}}{dt} \right) \tag{3.51}$$

3.13   Melting of Snow to Cloud Water and Rain, Simple Version

Snow can melt to cloud water and rain when snow exist at where temperature (T) is higher than freezing temperature (T_{freez}). The amount of snow melted per time step can be written as:

$$Psmlt' = \left(\frac{T - T_{freez}}{10} \right)^2 \frac{q_{snow}}{dt} \tag{3.52}$$

The melting process will stop when temperature reaches T_{freez} or all snow is melted:

$$Psmlt = \min \left(\frac{q_{snow}}{dt}, Psmlt', f_{s2r} \frac{c_{moist}}{L_{l2i}} \frac{T - T_{freez}}{dt} \right) \tag{3.53}$$

Note that the melting is scaled by a relaxation time f_{s2r}. Define $q_{mltsnow}$, maximum value of cloud water allowed from melted snow, exceed of which would be conversed to rain. It is used to prevent excessive cloud water. So the ratio of converted cloud water and total melted snow (ϵ) can be written as:

$$\epsilon = \min \left[1, \frac{\max \left(q_{mltsnow} - q_{water}, 0 \right)}{Psmlt \cdot dt} \right] \tag{3.54}$$

Thus, the ratio of converted rain and total melted snow is $1 - \epsilon$.

3.14   Melting of Snow to Cloud Water and Rain

Unlike the previous melting of snow to cloud water and rain process, which simply considers the temperature difference, here the snow melting considers the accretion between cloud water and snow, rain and snow. Snow

starts to melt when the temperature (T) is higher than the freezing temperature (T_{freez}). The calculation of melted snow follows Equation (32) in Lin et al. (1983):

$$Psmlt' = -\frac{2\pi}{\rho L_{l2s}} \left[K_a \left(T - T_{freez} \right) - L_{v2l} \psi \rho \left(q_{s2} - q_{vapor} \right) \right] n_{snow,0}$$
$$\left[0.78 \lambda_{snow}^{-2} + 0.31 S_c^{1/3} \Gamma \left(\frac{d+5}{2} \right) c^{1/2} \left(\frac{\rho_{sfc}}{\rho} \right)^{1/4} \nu^{-1/2} \lambda_{snow}^{-(d+5)/2} \right]$$
$$- \frac{c_{liquid} \left(T - T_{freez} \right)}{L_{l2s}} \left(Psacw + Psacr \right) \quad (3.55)$$

Melting of snow will stop when all snow has been melted, temperature (T) reaches freezing temperature (T_{freez}):

$$Psmlt = \min \left[\frac{q_{snow}}{dt}, \max \left(0, Psmlt' \right) + Pracs, \frac{c_{moist}}{L_{l2s}} \frac{T - T_{freez}}{dt} \right] \quad (3.56)$$

Define $q_{mltsnow}$, the maximum value of cloud water allowed from melted snow, exceed of which would be conversed to rain. It is used to prevent excessive cloud water. So the ratio of converted cloud water and total melted snow (ϵ) can be written as:

$$\epsilon = \min \left[1, \frac{\max \left(q_{mltsnow} - q_{water}, 0 \right)}{Psmlt \cdot dt} \right] \quad (3.57)$$

Thus, the ratio of converted rain and total melted snow is $1 - \epsilon$.

3.15   Melting of Graupel to Rain

Graupel melting considers the accretion between cloud water and graupel, rain and graupel. graupel starts to melt when the temperature (T) is higher than the freezing temperature (T_{freez}). The calculation of melted graupel follows Equation (47) in Lin et al. (1983):

$$Pgmlt' = -\frac{2\pi}{\rho L_{l2s}} \left[K_a \left(T - T_{freez} \right) - L_{v2l} \psi \rho \left(q_{s2} - q_{vapor} \right) \right] n_{graupel,0}$$
$$\left[0.78 \lambda_{graupel}^{-2} + 0.31 S_c^{1/3} \Gamma \left(\frac{f+5}{2} \right) e^{1/2} \left(\frac{4 g \rho_{graupel}}{3 C_D \rho} \right)^{1/4} \nu^{-1/2} \lambda_{graupel}^{-(f+5)/2} \right]$$
$$- \frac{c_{liquid} \left(T - T_{freez} \right)}{L_{l2s}} \left(Pgacw + Pgacr \right) \quad (3.58)$$

Melting of graupel will stop when all graupel has been melted, temperature (T) reaches freezing temperature (T_{freez}):

$$Pgmlt = \min \left[\frac{q_{graupel}}{dt}, \max \left(0, Pgmlt' \right), \frac{c_{moist}}{L_{l2s}} \frac{T - T_{freez}}{dt} \right] \quad (3.59)$$

3.16   Freezing of Rain to Graupel, Simple Version

Since rain is bigger than cloud water, freezing of rain will become graupel when rain exists at where temperature (T) is lower than freezing temperature (T_{freez}). The amount of rain frozen to graupel per time step

can be written as:

$$Pgfr' = \left(\frac{T - T_{freez}}{40}\right)^2 \frac{q_{rain}}{dt} \tag{3.60}$$

The freezing process stops when the temperature reaches T_{freez} or all rain is frozen:

$$Pgfr = \min\left(\frac{q_{rain}}{dt}, Pgfr', -f_{r2g}\frac{c_{moist}}{L_{l2i}}\frac{T - T_{freez}}{dt}\right) \tag{3.61}$$

Note that the freezing is scaled by a relaxation time f_{r2g}.

3.17   Freezing of Rain to Graupel

Unlike the previous freezing of rain to graupel process, which simply considers the temperature difference, freezing here is based on the work or Bigg (1953) and represents the formation of hail from raindrops due to immersion freezing. Freezing of rain to graupel starts when rain exists at where temperature (T) is lower than freezing temperature (T_{freez}). Calculation of freezing rain follows Equation (45) in Lin et al. (1983):

$$Pgfr = 20\pi^2 B' n_{rain,0}\left(\frac{\rho_{water}}{\rho}\right)\{\exp\left[-A'\left(T - T_{freez}\right)\right] - 1\}\lambda_{rain}^{-7} \tag{3.62}$$

3.18   Autoconversion from Cloud Water to Rain, Simple Version

Autoconversion is straightforward. Autoconversion of cloud water to rain is done when q_{water} excceds $q_{maxwater}$, maximum mass mixing ratio of cloud water for autoconversion of cloud water. So the amount of cloud water conversed to rain per time step can be written as:

$$Praut = f_{w2r}\frac{q_{water} - q_{maxwater}}{dt} \tag{3.63}$$

Note that autoconversion is scaled by the relaxation time f_{w2r}.

3.19   Autoconversion from Cloud Water to Rain

Unlike the previous autoconversion process, which uses a fixed threshold to trigger the conversion, here the autoconversion is done completely, autoconversion scales the threshold with subgrid variability and considers the cloud droplet number concentration. Before the vertical subgrid variability (z_{var}) is used in autoconversion of cloud water to rain, it is constrained by cloud water and a basic value:

$$z_{var} = \min\left[\max\left(q_{mincond}, z_{var}\right), 0.5q_{water}\right] \tag{3.64}$$

Autoconversion of cloud water to rain starts when the temperature (T) is higher than T_{wfr} follows Equations (16) and (17) in Hong et al. (2004), Equations (A38) and (A39) in Hong and Lim (2006), with subgrid

variability:

$$q_{crtwater} = \frac{4}{3}\pi\rho_{rain}r_{thresh}^3\frac{N_c}{\rho} \qquad (3.65)$$

$$dq = \min\left[1, \frac{H\left(q_{water} + z_{var} - q_{crtwater}\right)}{z_{var}}\right] \qquad (3.66)$$

$$Praut = \frac{0.104gE_{raut}\rho^{4/3}}{\mu\left(N_c\rho_{water}\right)^{1/3}}q_{water}^{7/3}dq \qquad (3.67)$$

where T_{wfr} is the minimum temperature water can exist (Moore and Molinero, 2011). H is the Heaviside unit step function (here set to 0.5 because subgrid variability is considered), which suppresses the autoconversion processes until cloud water reaches the critical mixing ratio ($q_{crtwater}$). E_{raut} is autoconversion efficiency from cloud water to rain. μ is the dynamic viscosity of air. r_{thresh} is critical cloud drop radius. Note that dq is revised using subgrid variability. If $q_{crtwater} = q_{water} + z_{var}$, $dq = 2H$; If $q_{crtwater} = q_{water}$, $dq = H$; If $q_{crtwater} = q_{water} - z_{var}$, $dq = 0.0$. If $q_{crtwater}$ from $q_{water} + z_{var}$ to $q_{water} - z_{var}$, it is linearly decaying from $2H$ to 0. There is an option not to use subgrid variability, dq is simplified to:

$$dq = q_{water} - q_{crtwater} \qquad (3.68)$$

3.20   Autoconversion from Cloud Ice to Snow, Simple Version

Autoconversion of cloud ice to snow is done when q_{ice} exceeds q_{maxice}, maximum mass mixing ratio cloud ice for autoconversion of cloud ice. This value follows Equation (15) in Hong et al. (2004). So the amount of cloud ice conversed to snow per time step can be written as

$$Psaut = f_{i2s}\frac{q_{ice} - q_{maxice}\dfrac{\rho_0}{\rho}}{dt} \qquad (3.69)$$

Note that autoconversion is scaled by the relaxation time f_{i2s}.

3.21   Autoconversion from Cloud Ice to Snow

Unlike the previous autoconversion process, which uses a fixed threshold to trigger the conversion, here the autoconversion is done completely, autoconversion scales the threshold with subgrid variability. In the future, autoconversion from cloud ice to snow needs to consider the number concentration of ice crystal (N_{ice} or N_i). There are several cloud ice to snow autoconversion schemes described in Straka (2009) that include the cloud ice number concentration. Before the vertical subgrid variability (z_{var}) is used in autoconversion of cloud ice to snow, it is constrained by $q_{minrain}$, the minimum value of rain:

$$z_{var} = \max\left(z_{var}, q_{minrain}\right) \qquad (3.70)$$

Autoconversion of cloud ice to snow is similar to Equation (21) in Lin et al. (1983), but with revision using subgrid variability. Define the upper bound (q_{plus}) and lower bound (q_{minus}) of subgrid variability of cloud ice:

$$q_{plus} = q_{ice} + z_{var} \qquad (3.71)$$

$$q_{minus} = q_{ice} - z_{var} \qquad (3.72)$$

Autoconversion starts when the temperature (T) is lower than freezing temperature (T_{freez}), and $q_{plus} - q_{minrain}$ exceeds autoconversion threshold (q_{autice}/ρ). The amount of autoconversion from cloud ice to snow per time step is written as:

$$Psaut = f_{i2s}E_{saut}\frac{0.25\left(q_{plus} - q_{autice}\dfrac{\rho_0}{\rho}\right)^2}{z_{var}\cdot dt}, \quad \text{if } q_{autice}\frac{\rho_0}{\rho} > q_{minus} \tag{3.73}$$

$$Psaut = f_{i2s}E_{saut}\frac{q_{ice} - q_{autice}\dfrac{\rho_0}{\rho}}{dt}, \quad \text{if } q_{autice}\frac{\rho_0}{\rho} \le q_{minus} \tag{3.74}$$

where q_{autice} is dependent on horizontal resolution. Note that if $q_{autice}/\rho = q_{plus}$, $Psaut = 0$; If $q_{autice}/\rho = q_{ice}$, $Psaut = 0.25f_{i2s}E_{saut}z_{var}/dt$; If $q_{autice}/\rho = q_{minus}$, $Psaut = f_{i2s}E_{saut}z_{var}/dt$. If q_{autice}/ρ from q_{plus} to q_{minus}, $Psaut$ cubicaly increases from 0 to $f_{i2s}E_{saut}z_{var}/dt$. E_{saut} is autoconversion efficiency. In GFDL MP, there are two types of terminal fall velocity: one is constant terminal fall velocity, the other is empirical terminal fall velocity. Terminal fall velocity can affect the autoconversion efficiency:

$$E_{saut} = \begin{cases} \exp\left[0.025\left(T - T_{freez}\right)\right], & \text{if variable fall} \\ 1, & \text{if constant fall} \end{cases} \tag{3.75}$$

In the end, the sum of accretion of cloud ice by snow and autoconversion should be less than 75% of total cloud ice.

3.22   Autoconversion from Snow to Graupel

When the temperature (T) is below the freezing temperature (T_{freez}), and snow exists, snow can autoconvert to graupel. Autoconversion of snow to graupel follows Equations (37) and (38) in Lin et al. (1983) when q_{snow} exceeds the threshold $q_{autsnow}/\rho$:

$$\alpha_{gaut} = 1 \times 10^{-3}\exp\left[0.09\left(T - T_{freez}\right)\right]dt \tag{3.76}$$

$$Pgaut = \min\left[\frac{q_{snow}}{dt}, Pgacs + \frac{\alpha_{gaut}}{1 + \alpha_{gaut}}\frac{q_{snow} - q_{autsnow}\dfrac{\rho_0}{\rho}}{dt}\right] \tag{3.77}$$

Autoconversion will stop when all snow are converted or the mass mixing ratio of snow is less than the autoconversion threshold.

3.23   Accretion of Cloud Water by Rain

After evaporation of rain, when cloud water and rain exists, and water vapor is saturated $(q_{minus} > q_{s0})$, do accretion of cloud water by rain following Equation (51) in Lin et al. (1983). The amount of cloud water accreted to rain per time step can be written as:

$$\alpha_{racw} = \frac{\pi E_{racw}n_{rain,0}a\Gamma\left(3 + b\right)}{4\lambda_{rain}^{3+b}}\left(\frac{\rho_{sfc}}{\rho}\right)^{1/2}dt \tag{3.78}$$

$$Pracw = \frac{\alpha_{racw}}{1 + \alpha_{racw}}\frac{q_{water}}{dt} \tag{3.79}$$

where E_{racw} is the collection efficiency. Here an implicit form $(q^{n+1} - q^n = -\alpha q^{n+1})$ is used.

3.24   Accretion of Cloud Water by Snow

Accretion of cloud water by snow starts when the temperature (T) is above freezing temperature (T_{freez}), and snow and cloud water exist. The calculation of accretion follows Equations (24) in Lin et al. (1983):

$$\alpha_{sacw} = \frac{\pi E_{sacw} n_{snow,0} c \Gamma \left(3+d\right)}{4\lambda_{snow}^{3+d}} \left(\frac{\rho_{sfc}}{\rho}\right)^{1/2} dt \tag{3.80}$$

$$Psacw = \frac{\alpha_{sacw}}{1+\alpha_{sacw}} \frac{q_{water}}{dt} \tag{3.81}$$

where E_{sacw} is the collection efficiency. The amount of water accreted by snow is written in implicit form.

3.25   Accretion of Rain by Snow

Accretion of rain by snow starts when the temperature (T) is above freezing temperature (T_{freez}), and snow and rain exist. The calculation of accretion follows Equations (28) in Lin et al. (1983):

$$Psacr' = \pi^2 E_{sacr} n_{snow,0} n_{rain,0} \left|v_{snow} - v_{rain}\right| \left(\frac{\rho_{rain}}{\rho}\right)$$
$$\left(\frac{5}{\lambda_{rain}^6 \lambda_{snow}} + \frac{2}{\lambda_{rain}^5 \lambda_{snow}^2} + \frac{0.5}{\lambda_{rain}^4 \lambda_{snow}^3}\right) \tag{3.82}$$

where E_{sacr} is the collection efficiency. v_{snow} and v_{rain} are the terminal fall velocity of snow and rain. The accretion will stop when all rain has been accreted:

$$Psacr = \min\left(Psacr', \frac{q_{rain}}{dt}\right) \tag{3.83}$$

3.26   Accretion of Snow by Rain

Accretion of snow by rain starts when the temperature (T) is above freezing temperature (T_{freez}), and snow and rain exist. The calculation of accretion follows Equations (27) in Lin et al. (1983):

$$Pracs = \pi^2 E_{racs} n_{rain,0} n_{snow,0} \left|v_{rain} - v_{snow}\right| \left(\frac{\rho_{snow}}{\rho}\right)$$
$$\left(\frac{5}{\lambda_{snow}^6 \lambda_{rain}} + \frac{2}{\lambda_{snow}^5 \lambda_{rain}^2} + \frac{0.5}{\lambda_{snow}^4 \lambda_{rain}^3}\right) \tag{3.84}$$

Where E_{racs} is the collection efficiency.

3.27   Accretion of Cloud Water by Graupel

Accretion of cloud water by graupel starts when the temperature (T) is above freezing temperature (T_{freez}), and graupel and cloud water exist. The calculation of accretion follows Equations (40) in Lin et al. (1983):

$$\alpha_{gacw} = \frac{\pi E_{gacw} n_{graupel,0} e \Gamma \left(3+f\right)}{4\lambda_{graupel}^{3+f}} \left(\frac{4g\rho_{graupel}}{3C_D \rho}\right)^{1/2} dt \tag{3.85}$$

$$Pgacw = \frac{\alpha_{gacw}}{1+\alpha_{gacw}} \frac{q_{water}}{dt} \tag{3.86}$$

Where E_{gacw} is the collection efficiency. The amount of cloud water accreted by graupel is written in implicit form.

3.28 Accretion of Rain by Graupel

Accretion of rain by graupel starts when the temperature (T) is above freezing temperature (T_{freez}), and graupel and rain exist. The calculation of accretion follows Equations (42) in Lin et al. (1983):

$$Pgacr' = \pi^2 E_{gacr} n_{graupel,0} n_{rain,0} \left| v_{graupel} - v_{rain} \right| \left(\frac{\rho_{rain}}{\rho} \right)$$
$$\left(\frac{5}{\lambda_{rain}^6 \lambda_{graupel}} + \frac{2}{\lambda_{rain}^5 \lambda_{graupel}^2} + \frac{0.5}{\lambda_{rain}^4 \lambda_{graupel}^3} \right) \quad (3.87)$$

Where E_{gacr} is the collection efficiency. $v_{graupel}$ is the terminal velocity of graupel. The accretion will stop when all rain has been accreted

$$Pgacrdt = \min \left(Pgacr', \frac{q_{rain}}{dt} \right) \quad (3.88)$$

3.29 Accretion of Cloud Ice by Snow

Accretion of cloud ice by snow starts when the temperature (T) is below freezing temperature (T_{freez}), and snow and cloud ice exist. The calculation of accretion follows Equations (22) in Lin et al. (1983):

$$E_{saci} = \exp \left[0.02 \left(T - T_{freez} \right) \right] \quad (3.89)$$

$$\alpha_{saci} = \frac{\pi E_{saci} n_{snow,0} c \Gamma (3+d)}{4 \lambda_{snow}^{3+d}} \left(\frac{\rho_{sfc}}{\rho} \right)^{1/2} dt \quad (3.90)$$

$$Psaci = \frac{\alpha_{saci}}{1 + \alpha_{saci}} \frac{q_{ice}}{dt} \quad (3.91)$$

where E_{saci} is the collection efficiency.The amount of cloud ice accreted by snow is written in implicit form.

3.30 Accretion of Cloud Ice by Graupel

Accretion of cloud ice by graupel starts when the temperature (T) is below freezing temperature (T_{freez}), and graupel and cloud ice exist. The calculation of accretion follows Equations (41) in Lin et al. (1983):

$$\alpha_{gaci} = \frac{\pi E_{gaci} n_{graupel,0} e \Gamma (3+f)}{4 \lambda_{graupel}^{3+f}} \left(\frac{4 g \rho_{graupel}}{3 C_D \rho} \right)^{1/2} \quad (3.92)$$

$$Pgaci = \frac{\alpha_{gaci}}{1 + \alpha_{gaci}} \frac{q_{ice}}{dt} \quad (3.93)$$

where E_{saci} is the collection efficiency.The amount of cloud ice accreted by graupel is written in implicit form.

3.31   Scaler for Accretion of Rain by Snow and Freezing of Rain to Graupel

In GFDL MP, there is a combined scaler for accretion of rain by snow and freezing of rain to graupel processes:

$$f_{r2s2g} = \frac{\min\left(Psacr + Pgfr, \dfrac{q_{rain}}{dt}, -\dfrac{c_{moist}}{L_{l2s}}\dfrac{T - T_{freez}}{dt}\right)}{\max\left(Psacr + Pgfr, \dfrac{q_{minrain}}{dt}\right)} \tag{3.94}$$

3.32   Accretion of Snow by Graupel

Accretion of snow by graupel starts when the temperature (T) is below freezing temperature (T_{freez}), and graupel and snow exist. The calculation of accretion follows Equations (29) in Lin et al. (1983):

$$\begin{aligned}
Pgacs = \pi^2 E_{gacs} n_{snow,0} n_{graupel,0} \left|v_{graupel} - v_{snow}\right| \left(\frac{\rho_{snow}}{\rho}\right) \\
\left(\frac{5}{\lambda_{snow}^6 \lambda_{graupel}} + \frac{2}{\lambda_{snow}^5 \lambda_{graupel}^2} + \frac{0.5}{\lambda_{snow}^4 \lambda_{graupel}^3}\right)
\end{aligned} \tag{3.95}$$

where E_{gacs} is the collection efficiency.

4   Sedimentation and Precipitation

4.1   Terminal Fall Velocity

Terminal fall velocity is the fall speed of hydrometeor under the condition of balance between the buoyancy-corrected gravitation force and the drag force (Pruppacher and Klett, 2010). There are two types of terminal fall velocity algorithms designed in the GFDL MP, one is constant terminal fall velocity, the other is a function of size distribution, mass mixing ratio, or temperature. In this cloud microphysics scheme, water vapor doesn't fall, and the falling speed of cloud water is too small to take into account.

Constant Terminal Fall Velocity

The idea of constant fall speed comes from IFS's cloud microphysics scheme. In this IFS document (https://www.ecmwf.int/sites/default/files/elibrary/2018/18714-part-iv-physical-processes.pdf), it is said that with the potential for hydrometeors to settle through many model layers in a single time step, using a mass related fall speed formulation can lead to numerical 'shocks' when long time steps are necessary if the numerics of the process are not carefully formulated. Thus the fall speeds are set to a constant to avoid this. In this case, the terminal fall velocity of cloud ice, rain, snow, and graupel is constant (v_{ic}, v_{rc}, v_{sc}, and v_{gc}).

Variational Terminal Fall Velocity

In general, terminal fall velocities of the hydrometeors follow the power law (Lin et al., 1983; Pruppacher and Klett, 2010). Therefore, the terminal velocity for rain, snow, and graupel of diameter D are:

$$v_{rain} = aD^b \left(\frac{\rho_{sfc}}{\rho} \right)^{0.5} \tag{4.1}$$

$$v_{snow} = cD^d \left(\frac{\rho_{sfc}}{\rho} \right)^{0.5} \tag{4.2}$$

$$v_{graupel} = eD^f \left(\frac{\rho_{sfc}}{\rho} \right)^{0.5} \left(\frac{4g\rho_{graupel}}{3C_D\rho_{sfc}} \right)^{0.5} \tag{4.3}$$

Following Srivastava (1967), the mass-weighted mean terminal velocities can be derived as:

$$v_{rain} = f_{vr} \frac{a\Gamma\left(4+b\right)}{6\lambda_{rain}^b} \left[\min\left(10, \frac{\rho_{sfc}}{\rho} \right) \right]^{1/2} \tag{4.4}$$

$$v_{snow} = f_{vs} \frac{c\Gamma\left(4+d\right)}{6\lambda_{snow}^d} \left[\min\left(10, \frac{\rho_{sfc}}{\rho} \right) \right]^{1/2} \tag{4.5}$$

$$v_{graupel} = f_{vg} \frac{e\Gamma\left(4+f\right)}{6\lambda_{graupel}^f} \left[\min\left(10, \frac{\rho_{sfc}}{\rho} \right) \right]^{1/2} \left(\frac{4g\rho_{graupel}}{3C_D\rho_{sfc}} \right)^{1/2} \tag{4.6}$$

Since the size distribution of cloud ice is assumed to be uniform, the calculation of terminal fall velocity for cloud ice follows Deng and Mace (2008):

$$v_{ice} = f_{vi}0.01 \cdot 10^{\left[a'(T-T_{freez})^2 + b'(T-T_{freez}) + c' \right] \log_{10}\left(10^3 q_{ice}\rho \right) + d'(T-T_{freez}) + e'} \tag{4.7}$$

or follows Heymsfield and Donner (1990):

$$v_{ice} = f_{vi} 3.29 \left(\rho q_{ice}\right)^{0.16} \tag{4.8}$$

Here scaling factors (f_{vi}, f_{vr}, f_{vs}, and f_{vg}) are used to adjust the terminal fall velocities of cloud ice, rain, snow, and graupel. The maximum and minimum values (v_{maxvi} and v_{minvi}, v_{maxvr} and v_{minvr}, v_{maxvs} and v_{minvs}, v_{maxvg} and v_{minvg}) are used to prevent extreme terminal fall velocities of cloud ice, rain, snow, and graupel.

4.2   Implicit Falls of Hydrometeors

Terminal fall velocity determines how fast the hydrometeor falls. It is similar to the horizontal wind in advection. An advection scheme is needed to vertically downward transport hydrometeor. In the GFDL MP, a time-implicit monotonic scheme for sedimentation was developed by Shian-Jiann Lin in 2016. The analytic equation for the 1D downward transport of the cloud 'condensates density' Q (Q can be q_{ice}, q_{rain}, q_{snow}, or $q_{graupel}$), given the downward terminal velocity V (V can be v_{ice}, v_{rain}, v_{snow}, or $v_{graupel}$), can be written as:

$$\frac{\partial}{\partial t}Q + \frac{\partial}{\partial z}\left(VQ\right) = 0 \tag{4.9}$$

We seek to discretize the above without the usual CFL limitation. The simplest and yet effective method is a fully time implicit upwind wind discretization. The upwind discretization ensures the positivity of the mixing ratio $q = Q/\rho$:

$$\frac{Q_k^{n+1} - Q_k^n}{\Delta t} = \frac{V_k Q_k^{n+1}}{\delta z_k} - \frac{V_{k-1} Q_{k-1}^{n+1}}{\delta z_{k-1}} \tag{4.10}$$

where k is from model top to bottom. Note that the direction of V and z are different. $\delta z_k = z_{k+\frac{1}{2}} - z_{k-\frac{1}{2}} < 0$ From this equation, we can derive:

$$Q_k^{n+1} = \frac{Q_k^n - \frac{\Delta t V_{k-1}}{\delta z_{k-1}} Q_{k-1}^{n+1}}{1 - \frac{\Delta t V_k}{\delta z_k}} \tag{4.11}$$

The above equation can be converted to:

$$\frac{Q_k^{n+1}}{\delta z_k} = \frac{Q_k^n - \Delta t V_{k-1} \frac{Q_{k-1}^{n+1}}{\delta z_{k-1}}}{\delta z_k - \Delta t V_k} \tag{4.12}$$

Rewriting the above equation in term of mixing ratio, the integration starts from the top layer ($k = 1$) as follows. For $k = 1$:

$$\frac{q_1^{n+1} \delta p_1}{\delta z_1} = \frac{q_1^n \delta p_1}{\delta z_1 - \Delta t V_1} \tag{4.13}$$

Note that typically the 'terminal fall velocity' at the top layer is zero, so the mixing ratio there stays the same. The mixing ratios in the interior (including the bottom layer, $k = 2, kbot$) is then updated sequentially from top to bottom as follows. Do $k = 2, kbot$

$$\frac{q_k^{n+1} \delta p_k}{\delta z_k} = \frac{q_k^n \delta p_k - \Delta t V_{k-1} \frac{q_{k-1}^{n+1} \delta p_{k-1}}{\delta z_{k-1}}}{\delta z_k - \Delta t V_k} \tag{4.14}$$

End do where the mixing ratio q, air density ρ, and terminal (downward, positive) velocity V are defined at the layer center, and δz_k is the layer thickness. Δt is the time step size. This transport scheme is conservative, monotonic, and stable for big time step. Output mass fluxes at each layer bottom are the accumulated of species mass loss above.

$$m_k = \sum_{i=1}^{k} \delta p_i \left(q_i^n - q_i^{n+1} \right) \tag{4.15}$$

The bottom layer mass flux becomes precipitation (See Figure 4).

MODEL LAYERS: – – **MODEL LEVELS:** ——

$m_0 = 0$

$u_1, v_1, dp_1, q_1^n \to q_1^{n+1}$

u, v_2 u, v_1 $m_1 = dp_1(q_1^n - q_1^{n+1})$

u, v_{k-1} u, v_{k-2} $m_{k-2} = m_{k-3} + dp_{k-2}(q_{k-2}^n - q_{k-2}^{n+1})$

$u_{k-1}, v_{k-1}, dp_{k-1}, q_{k-1}^n \to q_{k-1}^{n+1}$

u, v_k u, v_{k-1} $m_{k-1} = m_{k-2} + dp_{k-1}(q_{k-1}^n - q_{k-1}^{n+1})$

$u_k, v_k, dp_k, q_k^n \to q_k^{n+1}$

u, v_{k+1} u, v_k $m_k = m_{k-1} + dp_k(q_k^n - q_k^{n+1})$

u, v_{Kmax} u, v_{Kmax-1} $m_{Kmax-1} = m_{Kmax-2} + dp_{Kmax-1}(q_{Kmax-1}^n - q_{Kmax-1}^{n+1})$

$u_{Kmax}, v_{Kmax}, dp_{Kmax}, q_{Kmax}^n \to q_{Kmax}^{n+1}$

$m_{Kmax} = m_{Kmax-1} + dp_{Kmax}(q_{Kmax}^n - q_{Kmax}^{n+1}) = Precipitation$

Figure 4: Schematic of implicit fall and momentum exchange between the neighbouring layers.

4.3   Lagrangian Falls of hydrometeors

The Lagrangian fall utilizes the same piecewise parabolic method that is used in the FV3 dynamical core's vertically-Lagrangian solver. Details of this method can be found in Chapter 5 of the public FV3 documentation (https://repository.library.noaa.gov/view/noaa/30725) (Harris et al., 2021)

4.4   Impact of Sedimentation on Momentum and Temperature

Momentum is exchanged when hydrometeors fall. In this process, momentum is always conservative. Horizontal and vertical velocity, as well as associated temperature, are updated after cloud microphysics. Meanwhile, the falling hydrometeors bring down the air temperature from the above layer.

Horizontal Velocity

As it is shown in Figure 4, falling of hydrometeors can bring down the wind speed above and bring up the wind speed below as a compensation. Take the zonal wind (u) as an example:

$$u_k^{n+1}\delta p_k = u_k^n \delta p_k + \alpha - \beta \tag{4.16}$$

where the transport of upper-layer wind down (α) and transport of present-layer wind up (β) are written as:

$$\alpha = m_{k-1} u_{k-1}^{n+1} \tag{4.17}$$

$$\beta = m_{k-1} u_k^{n+1} \tag{4.18}$$

m_k is the combined falling flux of all hydrometeors. Here the time-implicit form is used. This formula also applies to the meridional wind (v).

Vertical Velocity

The transportation of vertical wind is more complicated since it is mixed with the sedimentation of hydrometeor itself. Similar to the transport of zonal wind, falling of hydrometeors can bring down the wind speed above and bring up the wind speed below as a compensation:

$$w_k^{n+1}\delta p_k = w_k^n \delta p_k + \alpha - \beta \tag{4.19}$$

where the transport of upper-layer wind down (α) and transport of present-layer wind up (β) are written as:

$$\alpha = m_{k-1} w_{k-1}^{n+1} - m_{k-1} V_{k-1} \tag{4.20}$$

$$\beta = m_{k-1} w_k^{n+1} - m_k V_k \tag{4.21}$$

m_k is the falling flux of each hydrometeor. V is the terminal fall velocity of each hydrometeor.

Temperature

Energy transport is used instead of directly temperature transport to ensure energy conservation. Assume the kinetic energy in the falling condensates is negligible compared to the potential energy. Local thermal equilibrium is assumed, and the loss in potential energy is transformed into internal energy (to heat the whole grid box). Backward time-implicit upwind transport scheme is used:

$$\delta p_k c_{moist,k} T_k^{n+1} = \delta p_k c_{moist,k} T_k^n + \alpha - \beta \tag{4.22}$$

where the transport of upper-layer energy down (α) and transport of present-layer energy up (β) are written as:

$$\alpha = m_{k-1} c_* T_{k-1}^{n+1} \tag{4.23}$$

$$\beta = m_k c_* T_k^{n+1} - (m_k - m_{k-1}) c_* T_k^n - m_{k-1} g z_k \tag{4.24}$$

5   Diagnostic Output

5.1   Cloud Fraction

Cloud fraction is diagnosed inside the GFDL MP. Four options are available. The first one is originally designed for this cloud microphysics scheme using the subgrid variability. The second one follows Xu and Randall (1996). The third one follows Park et al. (2016). The fourth one follows Gultepe and Isaac (2007). The first one is the default option in the current cloud microphysics scheme.

Option I (GFDL Method)

This option uses subgrid variability theory and is similar to that in Le Trent and Li (1991). Cloud water, cloud ice, rain, snow, and graupel are considered for computing cloud fraction. Define a new air temperature, the liquid-frozen water temperature (T_{in}), by assuming all liquid-phase water is evaporated to water vapor and all solid-phase water is sublimated to water vapor:

$$T_{in} = \frac{c_{moist}T - L_v\left(q_{liquid} + q_{solid}\right) - L_f\left(q_{ice} + q_{snow} + q_{graupel}\right)}{c_{v,dry} + \left(q_{vapor} + q_{cond}\right)c_{v,vapor}} \tag{5.1}$$

T_{in} then is used to calculate the saturation mass mixing ratio (q_{sat}):

$$q_{sat} = \begin{cases} q_{s2}(T_{in}), & \text{if } T_{in} \leq T_{freez} - 40 \\ q_{sw}(T_{in}), & \text{if } T_{in} \geq T_{freez} \\ \alpha q_{s2}(T_{in}) + \beta q_{sw}(T_{in}), & \text{if } T_{freez} - 40 < T_{in} < T_{freez} \end{cases} \tag{5.2}$$

where α and β are the partitioning factors defined as:

$$\alpha = \begin{cases} \dfrac{q_{solid}}{q_{cond}}, & \text{if } q_{cond} > 3 \times 10^{-6} \\ \dfrac{T_{freez} - T_{in}}{40}, & \text{if } q_{cond} \leq 3 \times 10^{-6} \end{cases} \tag{5.3}$$

$$\beta = \begin{cases} \dfrac{q_{liquid}}{q_{cond}}, & \text{if } q_{cond} > 3 \times 10^{-6} \\ 1 - \dfrac{T_{freez} - T_{in}}{40}, & \text{if } q_{cond} \leq 3 \times 10^{-6} \end{cases} \tag{5.4}$$

Relative humidity (RH) is calculated considering all hydrometeors as they are all assumed to convert to water vapor as:

$$RH = \frac{q_{vapor} + q_{cond}}{q_{sat}} \tag{5.5}$$

When calculating cloud fraction, the subgrid linear distribution in the horizontal (h_{var}) is assumed. This is effectively a smoother for the binary cloud scheme. Cloud fraction occurs only when $RH > 0.75$ and $q_{cond} + q_{vapor} > 1 \times 10^{-6}$. The upper and lower bounds of total hydrometeors are written as:

$$q_{plus} = (1 + q_h)\left(q_{vapor} + q_{cond}\right) \tag{5.6}$$

$$q_{minus} = (1 - q_h)\left(q_{vapor} + q_{cond}\right), \tag{5.7}$$

where q_h is as defined in (3.9). Finally, the cloud fraction (CF) is calculated as:

$$CF = \begin{cases} 1.0, & \text{if } q_{sat} < q_{minus} \\ \dfrac{q_{plus} - q_{sat}}{q_{plus} - q_{minus}}, & \text{if } q_{minus} \leq q_{sat} \leq q_{plus} \\ 0.0, & \text{if } q_{sat} > q_{plus} \end{cases} \tag{5.8}$$

Finally, cloud fraction is constrained by a basic value (CF_{min}) and 1.0:

$$CF = \min\left[1.0 \max\left(CF_{min}, CF\right)\right] \tag{5.9}$$

Option II (Xu-Randall Method)

This option follows Xu and Randall (1996). It uses the same relative humidity (RH), thresholds, saturation mass mixing ratio (q_{sat}), and all hydrometeors as option I. Cloud fraction is calculated as:

$$CF = \begin{cases} 1.0, & \text{if } RH \geq 1.0 \\ RH^{0.25}\left\{1 - \exp\left[-\dfrac{100 q_{cond}}{(1-RH)^{0.49} q_{sat}^{0.49}}\right]\right\}, & \text{if } 0.65 < RH < 1.0 \\ 0.0, & \text{if } RH \leq 0.65 \end{cases} \tag{5.10}$$

Option III (Park Method)

This option follows Park et al. (2016). It simply considers the mass mixing ratio of all hydrometeors:

$$CF' = \frac{1}{50} \times \left[5.77 \times \left(100 - \frac{x}{1000}\right) \times (1000 q_{cond})^{1.07} + 4.82 \times \left(\frac{x}{1000} - 50\right) \times (1000 q_{cond})^{0.94}\right] \tag{5.11}$$

Here CF' is the cloud fraction for mixed-phase cloud. It is then adjusted by the ratio of liquid-phase water and solid-phase water:

$$CF = CF'\left(\frac{0.92}{0.96}\frac{q_{liquid}}{q_{cond}} + \frac{1.0}{0.96}\frac{q_{solid}}{q_{cond}}\right) \tag{5.12}$$

Option IV (Gultepe-Isaac Method)

This option follows Gultepe and Isaac (2007). It also simply considers the mass mixing ratio of all hydrometeors:

$$\gamma = \frac{1000 q_{cond}}{0.28 + (1000 q_{cond})^{0.49}} \tag{5.13}$$

$$CF_{10} = \begin{cases} 0.0, & \text{if } \gamma < 0.18 \\ -0.1754 + 0.9811\gamma - 0.2223\gamma^2 + 0.0104\gamma^3, & \text{if } 0.18 < \gamma < 2.0 \\ 1.0, & \text{if } \gamma > 2.0 \end{cases} \tag{5.14}$$

$$CF_{100} = \begin{cases} 0.0, & \text{if } \gamma < 0.12 \\ -0.0913 + 0.7213\gamma + 0.1060\gamma^2 - 0.0946\gamma^3, & \text{if } 0.12 < \gamma < 1.85 \\ 1.0, & \text{if } \gamma > 1.85 \end{cases} \tag{5.15}$$

$$CF = CF_{10} + \left(\log_{10} \frac{x}{1000} - 1 \right) (CF_{100} - CF_{10}) \tag{5.16}$$

where CF_{10} is the cloud fraction for 10-km resolution, and CF_{100} is the cloud fraction for 100-km resolution.

5.2   Radar Reflectivity

As it was mentioned in the previous sections, radar reflectivity is the six month of hydrometeor size distribution. Only rain, snow, and graupel, which follow exponential size distribution, are included for radar reflectivity diagnosed. Three radar reflectivity options were built in the GFDL MP. The first one follows Stoelinga (2005), the second one follows the revised Stoelinga (2005) scheme by Smith and Xue (Smith et al., 1975; Tong and Xue, 2005). The third one follows Rogers and Yau (1989). The first one is the default option in the current cloud microphysics scheme.

Option I (Stoelinga Method)

The code to calculate reflectivity was originally from Mark Stoelinga's dbzcalc.f (refer to https://ams.confex.com/ams/32Rad11Meso/techprogram/paper_97032.htm) from the RIP package, modified for use in the GFDL MP. Rain, snow, and graupel are considered to calculate reflectivity. The reflectivity factor of rain (f_{rain}), snow (f_{snow}), and graupel ($f_{graupel}$) is defined as

$$f_{rain} = \gamma \left(\frac{1}{\pi \rho_{rain}} \right)^{1.75} 10^{18} \tag{5.17}$$

$$f_{snow} = \alpha \gamma \left(\frac{1}{\pi \rho_{snow}} \right)^{1.75} \left(\frac{\rho_{snow}}{\rho_{rain}} \right)^2 10^{18} \tag{5.18}$$

$$f_{graupel} = \alpha \gamma \left(\frac{1}{\pi \rho_{graupel}} \right)^{1.75} \left(\frac{\rho_{graupel}}{\rho_{rain}} \right)^2 10^{18} \tag{5.19}$$

where $\gamma = 720$, $\alpha = 0.224$. If air temperature is higher than T_{freez}, compute factor for brightband, where snow or graupel particle scatters like liquid water ($\alpha = 0.224$) because it is assumed to have a liquid skin:

$$f_{snow} = \frac{f_{snow}}{\alpha} \tag{5.20}$$

$$f_{graupel} = \frac{f_{graupel}}{\alpha} \tag{5.21}$$

Therefore, the total equivalent reflectivity (dBZ) is written as:

$$dBZ = 10\log\left\{\max\left[0.01, f_{rain}\frac{(\rho q_{rain})^{1.75}}{n_{0r}^{0.75}} + f_{snow}\frac{(\rho q_{snow})^{1.75}}{n_{0s}^{0.75}} + f_{graupel}\frac{(\rho q_{graupel})^{1.75}}{n_{0g}^{0.75}}\right]\right\} \tag{5.22}$$

Vertically maximum equivalent reflectivity (dBZ_{max}) is written as:

$$dBZ_{max} = \max\left(-20, dBZ\right) \tag{5.23}$$

Option II (Smith-Tong-Xue Method)

This is a modification of the Stoelinga scheme to use parameters from Smith et al. (1975) and modified by Tong and Xue (2005), albeit we do not use the modified parameters for the graupel reflectivity. This reflectivity also considers rain, snow and graupel, with snow divided into wet snow and dry snow. The reflectivity factor of rain (f_{rain}), wet snow (f_{snoww}), dry snow (f_{snowd}), and graupel ($f_{graupel}$) is defined as:

$$f_{rain} = \gamma\left(\frac{1}{\pi\rho_{rain}}\right)^{1.75}10^{18} \tag{5.24}$$

$$f_{snoww} = \gamma\left(\frac{1}{\pi\rho_{snow}}\right)^{1.75}10^{18} \tag{5.25}$$

$$f_{snowd} = \alpha\gamma\left(\frac{1}{\pi\rho_{snow}}\right)^{1.75}\left(\frac{\rho_{snow}}{\rho_{ice}}\right)^{2}10^{18} \tag{5.26}$$

$$f_{graupel} = \gamma\left(\frac{1}{\pi\rho_{graupel}}\right)^{1.75}10^{18} \tag{5.27}$$

where $\gamma = 720$, $\alpha = 0.224$. If air temperature is higher than T_{freez}, snow is treated as wet snow because it is assumed to have a liquid skin. If air temperature is lower than T_{freez}, snow is treated as dry snow. Therefore, the total equivalent reflectivity (dBZ) is written as:

$$dBZ = 10\log\left\{\max\left[0.01, f_{rain}\frac{(\rho q_{rain})^{1.75}}{n_{0r}^{0.75}} + f_{snow}\frac{(\rho q_{snow})^{1.75}}{n_{0s}^{0.75}} + f_{graupel}\frac{(\rho q_{graupel})^{1.75}}{n_{0g}^{0.75}}\right]\right\} \tag{5.28}$$

Vertically maximum equivalent reflectivity (dBZ_{max})

$$dBZ_{max} = \max\left(-20, dBZ\right) \tag{5.29}$$

Option III (Rogers-Yau Method)

This one is follow Rogers and Yau (1989). Precipitation rate of rain (Pr_{rain}), snow (Pr_{snow}) and graupel ($Pr_{graupel}$) can be defined as

$$Pr_{rain} = \frac{\rho q}{\rho_{rain}} v_{rain} \tag{5.30}$$

$$Pr_{snow} = \frac{\rho q}{\rho_{snow}} v_{snow} \tag{5.31}$$

$$Pr_{graupel} = \frac{\rho q}{\rho_{graupel}} v_{graupel} \tag{5.32}$$

Therefore, the total equivalent reflectivity (dBZ) is written as:

$$Z_e = 200 \left[\left(3.6 \times 10^6 Pr_{rain} \right)^{1.6} + \left(3.6 \times 10^6 Pr_{snow} \right)^{1.6} + \left(3.6 \times 10^6 Pr_{graupel} \right)^{1.6} \right] \tag{5.33}$$

$$dbz = 10 \log_{10} \left\{ \max \left[0.01, Z_e \right] \right\} \tag{5.34}$$

Vertically maximum equivalent reflectivity (dBZ_{max})

$$dBZ_{max} = \max \left(-20, dBZ \right) \tag{5.35}$$

5.3   Cloud Effective Radius

The cloud effective radius connects the cloud microphysics and radiation. The size and distribution of hydrometeors significantly impact the radiation and the global energy balance. There are several options in the GFDL MP for cloud effective radius calculation. There are also options to decide whether liquid-phase water or solid-phase water should be combined.

The calculation of effective radius of cloud water (R_{water}) has two options. Option one assumes the cloud water is spherical following Martin et al. (1994):

$$R_{water} = \left(\frac{3\rho q_{water}}{4\pi \rho_{water} N_{water}} \right)^{1/3} 10^6 \tag{5.36}$$

N_{water} is the empirical number concentration of cloud water following the definition in Martin et al. (1994). By default, it uses the values of N_c from the GFDL MP. Option two considers the difference of land and ocean, and is simply a function of temperature following revised Kiehl (1994):

$$R'_{water} = 14(1 - LSM) + \left\{ 8 + 6 \min \left[1, \max \left(0, \frac{T_{freez} - T}{30} \right) \right] \right\} LSM \tag{5.37}$$

$$R_{water} = R'_{water} + (14 - R'_{water}) \min \left[1, \max \left(0, \frac{D_{snow}}{1000} \right) \right] \tag{5.38}$$

where D_{snow} is snow depth.

The calculation effective radius of cloud ice (R_{ice}) has five options. Option one is a function of cloud ice

content and temperature following Heymsfield and McFarquhar (1996):

$$R_{ice} = \begin{cases} \dfrac{\beta}{9.917} \left(\rho q_{ice} 10^3\right)^{0.109} 10^3, & \text{if } T < T_0 - 50 \\[2ex] \dfrac{\beta}{9.337} \left(\rho q_{ice} 10^3\right)^{0.080} 10^3, & \text{if } T_0 - 50 \leq T < T_0 - 40 \\[2ex] \dfrac{\beta}{9.208} \left(\rho q_{ice} 10^3\right)^{0.055} 10^3, & \text{if } T_0 - 40 \leq T < T_0 - 30 \\[2ex] \dfrac{\beta}{9.387} \left(\rho q_{ice} 10^3\right)^{0.031} 10^3, & \text{if } T \geq T_0 - 30 \end{cases}, \tag{5.39}$$

where $\beta = 1.22$. Option two is simply a function of temperature following Donner et al. (1997):

$$R_{ice} = \begin{cases} 15.41627, & \text{if } T - T_{freez} < -55 \\ 16.60895, & \text{if } -55 \leq T - T_{freez} < -50 \\ 32.89967, & \text{if } -50 \leq T - T_{freez} < -45 \\ 35.29989, & \text{if } -45 \leq T - T_{freez} < -40 \\ 55.65818, & \text{if } -40 \leq T - T_{freez} < -35 \\ 85.19071, & \text{if } -35 \leq T - T_{freez} < -30 \\ 72.35392, & \text{if } -30 \leq T - T_{freez} < -25 \\ 92.46298, & \text{if } T - T_{freez} \geq -25 \end{cases} \tag{5.40}$$

Option three is also a function of temperature following Fu (2007):

$$R_{ice} = 47.05 + 0.6624 \left(T - T_{freez}\right) + 0.001741 \left(T - T_{freez}\right)^2 \tag{5.41}$$

Option four is also a function of temperature following Kristjansson et al. (2000):

$$\alpha = \min\left\{\max\left[\left(INT\left(T - 136.0\right), 44\right], 138 - 1\right\}\right. \tag{5.42}$$

$$\beta = T - INT(T) \tag{5.43}$$

$$R_{ice} = \Lambda(\alpha)\left(1. - \beta\right) + \Lambda\left(\alpha + 1\right)\beta \tag{5.44}$$

where Λ is a prescribed discrete curve. Option five is a function of cloud ice content and temperature following Wyser (1998):

$$\beta = -2 + 10^{-3} \times \log_{10}\left(\frac{\rho q_{ice}}{\rho_0}\right)\left(T_{freez} - T\right)^{1.5} \tag{5.45}$$

$$R_{ice} = 377.4 + 203.3\beta + 37.91\beta^2 + 2.3696\beta^3 \tag{5.46}$$

Option six is a function of cloud ice content and temperature following Sun and Rikus (1999); Sun (2001):

$$R_{ice} = 45.8966 \times \left(\rho q_{ice} 10^3\right)^{0.2214} + 0.7957 \times \left(\rho q_{ice} 10^3\right)^{0.2535} \left(T - T_{freez} + 190.0\right) \tag{5.47}$$

$$R_{ice} = \left[1.2351 + 0.0105 \times \left(T - T_{freez}\right)\right] R_{ice} \tag{5.48}$$

The effective radii of rain (R_{rain}), snow (R_{snow}), and graupel ($R_{graupel}$) are derived from their size distri-

bution Lin et al. (1983):

$$R_{rain} = \frac{3}{2\lambda_{rain}} 10^6 \tag{5.49}$$

$$R_{snow} = \frac{3}{2\lambda_{snow}} 10^6 \tag{5.50}$$

$$R_{graupel} = \frac{3}{2\lambda_{graupel}} 10^6, \tag{5.51}$$

They can also be derived as the mass-weighted form from Lin et al. (1983):

$$R_{rain} = \frac{\left[\dfrac{\Gamma(4+b)}{6}\right]^{\frac{1}{b}}}{2\lambda_{rain}} 10^6 \tag{5.52}$$

$$R_{snow} = \frac{\left[\dfrac{\Gamma(4+d)}{6}\right]^{\frac{1}{d}}}{2\lambda_{snow}} 10^6 \tag{5.53}$$

$$R_{graupel} = \frac{\left[\dfrac{\Gamma(4+f)}{6}\right]^{\frac{1}{f}}}{2\lambda_{graupel}} 10^6, \tag{5.54}$$

The maximum and minimum values ($R_{maxrain}$ and $R_{minrain}$, $R_{maxsnow}$ and $R_{minsnow}$, $R_{maxgraupel}$ and $R_{mingraupel}$) are used to cap the range of radii of rain, snow, and graupel.

Appendix A   List of Symbols

Notation	Description	Value	Units
a	constant in empirical formula	842	$cm^{1-b}s^{-1}$
a'	constant in empirical formula v_{ice}	-4.14122×10^{-5}	
A	parameter in sublimation / deposition processes		sm^{-2}
A'	parameter in Bigg mechanism	0.66	K^{-1}
b	constant in empirical formula	0.8	
b'	constant in empirical formula v_{ice}	-0.00538922	
B	parameter in sublimation / deposition processes		sm^{-2}
B'	parameter in Bigg mechanism	100	$m^{-3}s^{-1}$
c	parameter to control snow to cloud water and snow to water vapor conversion	4.8	$cm^{1-d}s^{-1}$
c'	constant in empirical formula v_{ice}	-0.0516344	
c_*	heat capacity		$Jkg^{-1}K^{-1}$
c_{moist}	moist specific heat		$Jkg^{-1}K^{-1}$
c_{liquid}	liquid phase specific heat at T_{freez}	4218	$Jkg^{-1}K^{-1}$
$c_{p,dry}$	dry air specific heat at constant pressure	1004.6	$Jkg^{-1}K^{-1}$
$c_{p,liquid}$	liquid phase specific heat at constant pressure at T_{freez}	4218	$Jkg^{-1}K^{-1}$
$c_{p,moist}$	moist specific heat constant pressure		$Jkg^{-1}K^{-1}$
$c_{p,solid}$	solid phase specific heat at constant pressure at T_{freez}	2106	$Jkg^{-1}K^{-1}$
$c_{p,vapor}$	water vapor specific heat at constant pressure $(4R_{vapor})$	1846	$Jkg^{-1}K^{-1}$
c_{solid}	solid phase specific heat at T_{freez}	2106	$Jkg^{-1}K^{-1}$
$c_{v,dry}$	dry air specific heat at constant volume $(c_{p,dry} - R_{dry})$	717.55	$Jkg^{-1}K^{-1}$
$c_{v,liquid}$	liquid phase specific heat at constant volume at T_{freez}	4218	$Jkg^{-1}K^{-1}$
$c_{v,moist}$	moist specific heat constant volume		$Jkg^{-1}K^{-1}$
$c_{v,solid}$	solid phase specific heat at constant volume at T_{freez}	2106	$Jkg^{-1}K^{-1}$
$c_{v,vapor}$	water vapor specific heat at constant volume $(3R_{vapor})$	1384.5	$Jkg^{-1}K^{-1}$
c_{vapor}	water vapor specific heat		$Jkg^{-1}K^{-1}$
C	parameter in evaporation / condensation processes		sm^{-2}
C_D	drag coefficients for hail / graupel		
CF	cloud fraction		
CF'	cloud fraction for mixed-phase cloud		
CF_{10}	cloud fraction in 10-km resolution		
CF_{100}	cloud fraction in 100-km resolution		
CF_{min}	minimum cloud fraction	0.05	
d	constant in empirical formula	0.25	
dq	difference of hydrometeor mass mixing ratio		$kgkg^{-1}$
dp	pressure thickness of dry air (positive)		Pa
dp'	pressure thickness of moist air (positive)		Pa
dt	time step		s
dt_c	cloud microphysics time step		s
dt_{fr}	T_{wfr} - dt_{fr}: minimum temperature water can exist	8	K
dt_m	vertical remapping time step		s

dt_p	physics time step		s
dz	height thickness (negative)		m
dBZ	radar reflectivity		dBZ
dBZ_{max}	maximum radar reflectivity		dBZ
d'	constant in empirical formula v_{ice}	0.00216078	
D	parameter in evaporation / condensation processes		sm^{-2}
D_{land}	base value for subgrid deviation / variability over land	0.12	$km^{-1/2}$
D_{ocean}	base value for subgrid deviation / variability over ocean	0.08	$km^{-1/2}$
D_{snow}	snow depth		m
$\bar{D}_{conice}$	parameter in ice deposition	11.9	$mkg^{-0.5}$
e	constant in empirical formula	1	$cm^{1-b}s^{-1}$
e'	constant in empirical formula v_{ice}	1.9714	
e_0	saturation water vapor pressure at T_{freez}	611.21	Pa
e_{s0}	saturation water vapor pressure for the table N		Pa
e_{s1}	saturation water vapor pressure for the table I		Pa
e_{s2}	saturation water vapor pressure for the table II		Pa
e_{s3}	saturation water vapor pressure for the table III		Pa
e_{s4}	saturation water vapor pressure for the table IV		Pa
E_{gaci}	collection efficiency of cloud ice by graupel	0.05	
E_{gacr}	collection efficiency of rain by graupel	1	
E_{gacs}	collection efficiency of snow by graupel	0.01	
E_{gacw}	collection efficiency of cloud water by graupel	1	
E_{racs}	collection efficiency of snow by rain	1	
E_{racw}	collection efficiency of cloud water by rain	0.8	
E_{raut}	collection efficiency of cloud water to rain autoconversion	0.8	
E_{saci}	collection efficiency of cloud ice by snow		
E_{sacr}	collection efficiency of rain by snow	1	
E_{sacw}	collection efficiency of cloud water by snow	1	
E_{saut}	collection efficiency of cloud ice to snow autoconversion		
f	constant in empirical formula	0.5	
$f_{graupel}$	reflectivity factor of graupel		
f_{rain}	reflectivity factor of rain		
f_{snow}	reflectivity factor of snow		
f_{vg}	tunable factor for graupel fall	1	
f_{vi}	tunable factor for cloud ice fall	1	
f_{vr}	tunable factor for rain fall	1	
f_{vs}	tunable factor for snow fall	1	
f_{x2y}	conversion rate from hydrometeor x to hydrometeor y		
g	gravitational acceleration	9.80665	ms^{-2}
h_{var}	subgrid variability in horizontal direction		
H	Heaviside unit step function	0.5	
IE	internal energy		Jkg^{-1}
k	vertical index		

$kbot$	bottom layer index		
K_a	thermal conductivity of air	2.36×10^{-2}	$Jm^{-1}s^{-1}K^{-1}$
L	latent heat		Jkg^{-1}
L_f	latent heat of fusion at $0K$		Jkg^{-1}
L_{fus}	latent heat of fusion at T_{freez}	3.3358×10^5	Jkg^{-1}
L_{l2s}	true latent heat of melting / freezing		Jkg^{-1}
L_v	atent heat of condensation / evaporation at $0K$		Jkg^{-1}
L_{v2l}	true latent heat of condensation / evaporation		Jkg^{-1}
L_{v2s}	true latent heat of deposition / sublimation		Jkg^{-1}
L_{vap}	latent heat of evaporation at T_{freez}	2.5×10^6	Jkg^{-1}
L'_{v2l}	special latent heat of condensation / evaporation for saturated water vapor		Jkg^{-1}
LSM	land sea mask, 1: land, 0: sea		
m	sedimentation mass flux		Pa
M	mass		kg
M_{dry}	dry air mass		kg
$M_{graupel}$	graupel mass		kg
M_{ice}	cloud ice mass		kg
M_{rain}	rain mass		kg
M_{snow}	snow mass		kg
M_{vapor}	water vapor mass		kg
M_{water}	cloud water mass		kg
n	size distribution		m^{-4}
n_0	intercept parameter		m^{-4}
$n_{graupel}$	size distribution of graupel		m^{-4}
$n_{graupel,0}$	intercept parameter of graupel size distribution	4.0×10^6	m^{-4}
n_{hail}	size distribution of hail		m^{-4}
$n_{hail,0}$	intercept parameter of hail size distribution	4.0×10^4	m^{-4}
n_{rain}	size distribution of rain		m^{-4}
$n_{rain,0}$	intercept parameter of rain size distribution	8.0×10^6	m^{-4}
n_{snow}	size distribution of snow		m^{-4}
$n_{snow,0}$	intercept parameter of snow size distribution	3.0×10^6	m^{-4}
N_c	cloud droplet number concentration (CDNC)		m^{-3}
$N_{c,land}$	prescribed cloud droplet number concentration over land	300	cm^{-3}
$N_{c,ocean}$	prescribed cloud droplet number concentration over ocean	200	cm^{-3}
$N_{graupel}$	number concentration of graupel		m^{-3}
N_i	activated cloud ice number concentration		m^{-3}
N_{ice}	number concentration of cloud ice		m^{-3}
N_{rain}	number concentration of rain		m^{-3}
N_{snow}	number concentration of snow		m^{-3}
N_{water}	number concentration of cloud water		m^{-3}
p	air pressure		Pa
p_{int}	interface air pressure		Pa

$Pr_{graupel}$	graupel precipitation rate		ms^{-1}
Pr_{rain}	rain precipitation rate		ms^{-1}
q	hydrometeor mass mixing ratio		$kgkg^{-1}$
q'	hydrometeor specific ratio		$kgkg^{-1}$
$q_{aerosol}$	aerosol mass mixing ratio		$kgkg^{-1}$
q_{autice}	ice to snow density autoconversion threshold	8×10^{-5}	$kgkg^{-3}$
$q_{autsnow}$	snow to graupel density autoconversion threshold	1×10^{-3}	$kgkg^{-3}$
q_{cond}	total water condensate mass mixing ratio		$kgkg^{-1}$
q_{crtice}	initial ice nuclei mass mixing ratio		$kgkg^{-1}$
$q_{crtwater}$	critical mass mixing ratio for cloud water in autoconversion		$kgkg^{-1}$
q_{genice}	maximum cloud ice generated during remapping step	1.82×10^{-6}	$kgkg^{-1}$
$q_{genwater}$	maximum cloud water generated during remapping step	1×10^{-3}	$kgkg^{-1}$
$q_{graupel}$	graupel mixing ratio		$kgkg^{-1}$
q_h	dispersion of hydrometeors		$kgkg^{-1}$
q_{hail}	hail mixing ratio		$kgkg^{-1}$
q_{ice}	cloud ice mixing ratio		$kgkg^{-1}$
q_{limice}	cloud ice limiter to prevent large ice build up	1	$kgkg^{-1}$
q_{liquid}	liquid phase water species mass mixing ratio		$kgkg^{-1}$
q_{maxice}	maximum cloud ice mass mixing ratio for autoconversion of cloud ice	1.0×10^{-4}	$kgkg^{-1}$
$q_{maxwater}$	maximum cloud water mass mixing ratio for autoconversion of cloud water	2×10^{-3}	$kgkg^{-1}$
$q_{mincond}$	minimum value for cloud condensates	1×10^{-12}	$kgkg^{-1}$
$q_{minrain}$	minimum value for rain	1×10^{-8}	$kgkg^{-1}$
q_{minus}	lower bound of the hydrometeors		$kgkg^{-1}$
$q_{minvapor}$	minimum value for water vapor	1×10^{-20}	$kgkg^{-1}$
$q_{mltsnow}$	maximum value of cloud water allowed from melted snow	1×10^{-6}	$kgkg^{-1}$
$q_{mltwater}$	maximum value of cloud water allowed from melted cloud ice	1×10^{-3}	$kgkg^{-1}$
q_{plus}	upper bound of the hydrometeors		$kgkg^{-1}$
q_{rain}	rain mixing ratio		$kgkg^{-1}$
q_{tmp}	a temporal variable to store mass mixing ratio		$kgkg^{-1}$
q_s	saturation specific humidity for the table I		$kgkg^{-1}$
q_{s2}	saturation specific humidity for the table III		$kgkg^{-1}$
q_{snow}	snow mixing ratio		$kgkg^{-1}$
q_{solid}	solid phase water species mass mixing ratio		$kgkg^{-1}$
q_{sw}	saturation specific humidity for the table II		$kgkg^{-1}$
q_{vapor}	water vapor mixing ratio		$kgkg^{-1}$
q_{water}	cloud water mixing ratio		$kgkg^{-1}$
Q	condensates density		kgm^{-3}
r	radius of hydrometeor		m
r_{thresh}	critical cloud drop radius	10×10^{-6}	$micro$

R_{dry}	dry air gas constant	287.05	$Jkg^{-1}K^{-1}$
$R_{graupel}$	graupel radius		$micron$
R_{ice}	cloud ice radius		$micron$
$R_{maxgraupel}$	maximum graupel radius		$micron$
R_{maxice}	maximum cloud ice radius		$micron$
$R_{maxrain}$	maximum rain radius		$micron$
$R_{maxsnow}$	maximum snow radius		$micron$
$R_{maxwater}$	maximum cloud water radius		$micron$
$R_{mingraupel}$	minimum graupel radius		$micron$
R_{minice}	minimum cloud ice radius		$micron$
$R_{minrain}$	minimum rain radius		$micron$
$R_{minsnow}$	minimum snow radius		$micron$
$R_{minwater}$	minimum cloud water radius		$micron$
R_{rain}	rain radius		$micron$
R_{snow}	snow radius		$micron$
R_{vapor}	water vapor gas constant	461.5	$Jkg^{-1}K^{-1}$
R_{water}	cloud water radius		$micron$
RH	relative humidity		
RH_{adj}	relative humidity threshold for complete evaporation / sublimation		
RH_{inc}	RH increment for complete evaporation / sublimation of cloud water / cloud ice	0.3	
RH_{inr}	RH increment for complete evaporation of rain	0.3	
RH_{rain}	relative humidity for rain		
RH_{revap}	relative humidity threshold for rain evaporation		
S_c	Schmidt number $= \nu/\psi$		
t	time		s
T	air temperature		K
T'	scaled air temperature for saturation table		K
T_{tmp}	temporal variable to store air temperature		K
T_{freez}	freezing temperature	273.16	K
T_{in}	liquid frozen temperature		K
T_{min}	minimum temperature for sublimation of cloud ice	178	K
T_{sub}	minimum temperature for sublimation of cloud ice	184	K
T_{wfr}	critical freezing temperature (T_{freez} - 40)	233.16	K
T_v	virtual temperature		K
u	zonal wind		ms^{-1}
v	meridional wind		ms^{-1}
v_{gc}	constant graupel fall speed	2	ms^{-1}
$v_{graupel}$	graupel fall speed		ms^{-1}
v_{ic}	constant cloud ice fall speed	1/3	ms^{-1}
v_{ice}	cloud ice fall speed		ms^{-1}
v_{rain}	rain fall speed		ms^{-1}
v_{rc}	constant rain fall speed	4	ms^{-1}
v_{sc}	constant snow fall speed	1	ms^{-1}

v_{snow}	snow fall speed		ms^{-1}
v_{maxvg}	maximum fall speed for graupel	12.0	ms^{-1}
v_{maxvi}	maximum fall speed for cloud ice	1.0	ms^{-1}
v_{maxvr}	maximum fall speed for rain	12	ms^{-1}
v_{maxvs}	maximum fall speed for snow	6.0	ms^{-1}
v_{minvg}	minimum fall speed for graupel	1×10^{-5}	ms^{-1}
v_{minvi}	minimum fall speed for cloud ice	1×10^{-5}	ms^{-1}
v_{minvr}	minimum fall speed for rain	1×10^{-3}	ms^{-1}
v_{minvs}	minimum fall speed for snow	1×10^{-5}	ms^{-1}
V	terminal velocity		ms^{-1}
w	vertical velocity		ms^{-1}
x	grid size		m
z	height		m
z_{int}	interface height		m
z_{var}	subgrid variability in vertical direction		
z_{vir}	ratio of the gas constants of dry air and water vapor $(R_{vapor}/R_{dry} - 1)$	0.6077338443	
Z_e	radar reflectivity factor		$mm^6 m^{-3} \mu m^3$
χ	diffusivity of water vapor in air	2.26×10^{-5}	$m^2 s^{-1}$
Δq	mass mixing ratio increment		$kg kg^{-1}$
ΔT	temperature increment		K
Γ	gamma function		
λ	slope parameter		cm^{-1}
$\lambda_{graupel}$	slope parameter in graupel size distribution		cm^{-1}
λ_{rain}	slope parameter in rain size distribution		cm^{-1}
λ_{snow}	slope parameter in snow size distribution		cm^{-1}
μ	dynamic viscosity of air	1.717×10^{-5}	$kg m^{-1} s^{-1}$
ν	kinematic viscosity of air	1.259×10^{-5}	$cm^2 s^{-1}$
π	ratio of a circle's circumference to its diameter	3.1415926535897931	
ψ	diffusivity of water vapor in air	2.11×10^{-5}	$cm^2 s^{-1}$
ρ	air density		$kg m^{-3}$
ρ_0	reference air density	1.0	$kg m^{-3}$
ρ_{bot}	bottom layer air density		$kg m^{-3}$
$\rho_{graupel}$	density of graupel	4×10^2	$kg m^{-3}$
ρ_{hail}	density of hail	9.17×10^2	$kg m^{-3}$
ρ_{rain}	density of rain	1×10^3	$kg m^{-3}$
ρ_{sfc}	surface air density	1.2	$kg m^{-3}$
ρ_{snow}	density of snow	1×10^2	$kg m^{-3}$
ρ_{water}	density of cloud water	1×10^3	$kg m^{-3}$
τ_{x2y}	relaxation time scale from hydrometeor x to hydrometeor y		s

Appendix B   List of Constants in IFS

Notation	Description	Value	Units
R_E	Earth radius	6371229	m
c_{light}	speed of light in vacuum	299792458	ms^{-1}
$c_{p,dry}$	dry air specific heat at constant pressure $(7/2R_{dry})$	1004.7090	$Jkg^{-1}K^{-1}$
$c_{p,liquid}$	liquid phase specific heat at constant pressure at T_{freez}	4218	$Jkg^{-1}K^{-1}$
$c_{p,solid}$	solid phase specific heat at constant pressure at T_{freez}	2106	$Jkg^{-1}K^{-1}$
$c_{p,vapor}$	water vapor specific heat at constant pressure $(4R_{vapor})$	1846.1	$Jkg^{-1}K^{-1}$
$c_{v,dry}$	dry air specific heat at constant volume $(5/2R_{dry})$	717.6493	$Jkg^{-1}K^{-1}$
$c_{v,liquid}$	liquid phase specific heat at constant volume at T_{freez}	4218	$Jkg^{-1}K^{-1}$
$c_{v,solid}$	solid phase specific heat at constant volume at T_{freez}	2106	$Jkg^{-1}K^{-1}$
$c_{v,vapor}$	water vapor specific heat at constant volume $(3R_{vapor})$	1384.575	$Jkg^{-1}K^{-1}$
g	gravitational acceleration	9.80665	ms^{-2}
h	Planck constant	$6.6260755 \times 10^{-34}$	Js
K	Boltzmann constant	1.380658×10^{-23}	JK^{-1}
L_{fus}	latent heat of fusion at T_{freez}	3.337×10^5	Jkg^{-1}
L_{vap}	latent heat of evaporation at T_{freez}	2.5008×10^6	Jkg^{-1}
m_{dry}	dry air molar mass	28.9644×10^{-3}	$kgmol^{-1}$
m_{vapor}	water vapor molar mass	18.0153×10^{-3}	$kgmol^{-1}$
N	Avogadro number	6.0221367×10^{23}	mol^{-1}
R	universal gas constant (NK)	8.31451	$JK^{-1}mol^{-1}$
R_{dry}	dry air gas constant (R/m_{dry})	287.0597	$Jkg^{-1}K^{-1}$
R_{vapor}	water vapor gas constant (R/m_{vapor})	461.5250	$Jkg^{-1}K^{-1}$
S_0	total solar irradiance	1370	Wm^{-2}
T_{freez}	freezing temperature	273.16	K
z_{vir}	ratio of the gas constants of dry air and water vapor $(R_{vapor}/R_{dry} - 1)$	0.6078	
σ	Stefan-Boltzmann constant $(\frac{2\pi^5 K^4}{15c_{light}^2 h^3})$	5.6705085×10^{-8}	$Wm^{-2}K^{-4}$

Data in this table is obtained from the IFS documentation: https://www.ecmwf.int/en/elibrary/18714-ifs-documentation-cy45r1-part-iv-physical-processes

Appendix C Namelist Guide

C.1 General

mp_time

Real: Sub time step of the GFDL MP. If **mp_time** isn't divisible by physics time step or is larger than physics time step, the actual MP time step becomes $dt/\mathrm{NINT}[dt/\mathrm{MIN}(dt, mp\_time)]$. The unit is s. 150 by default.

ntimes

Integer: Sub cycle times in the GFDL MP. It used to divide the remapping time step or physics time step. 1 by default.

fix_negative

Logical: Set $.true.$ to fix negative hydrometeors using other hydrometeors or nearby points. $.true.$ as default.

consv_checker

Logical: Set $.true.$ to activate the total energy and total water checker. $.false.$ by default.

C.2 Conversion Time Scale

tau_v2l

Real: Time scale for cloud water condensation. Increasing / decreasing **tau_v2l** can slow down / speed up cloud water condensation (water vapor → cloud water). The unit is s. 150 by default.

tau_l2v

Real: Time scale for cloud water evaporation. Increasing / decreasing **tau_l2v** can slow down / speed up cloud water evaporation (cloud water → water vapor). The unit is s. 300 by default.

tau_l2r

Real: Time scale for autoconversion of cloud water to rain. Increasing / decreasing **tau_l2r** can slow down / speed up autoconversion of cloud water to rain (cloud water → rain). The unit is s. 900 by default.

tau_r2g

Real: Time scale for freezing of rain to graupel. Increasing / decreasing **tau_r2g** can slow down / speed up freezing of rain to graupel (rain → graupel). The unit is s. 900 by default.

tau_i2s

Real: Time scale for autoconversion of cloud ice to snow. Increasing / decreasing **tau_i2s** can slow down / speed up autoconversion of cloud ice to snow (cloud ice → snow). The unit is s. 1000 by default.

tau_imlt

Real: Time scale for cloud ice melting. Increasing / decreasing **tau_imlt** can slow down / speed up melting of cloud ice to cloud water or rain (cloud ice → cloud water or rain). The unit is s. 1200 by default.

tau_smlt

Real: Time scale for snow melting. Increasing / decreasing **tau_smlt** can slow down / speed up melting of snow to cloud water or rain (snow → cloud water or rain). The unit is s. 900 by default.

tau_gmlt

Real: Time scale for graupel melting. Increasing / decreasing **tau_g2r** can slow down / speed up melting of graupel to rain (graupel → rain). The unit is s. 600 by default.

tau_revp

Real: Time scale for rain evaporation. Increasing / decreasing **tau_g2r** can slow down / speed up rain evaporation (rain → water vapor). The unit is s. 0 by default.

C.3   Subgrid Variability

dw_land

Real: Basic value for subgrid variability over land. 0.2 by default.

dw_ocean

Real: Basic value for subgrid variability over ocean. 0.1 by default.

z_slope_liq

Logical: Set *.true.* to turn on vertically subgrid linear monotonic slope for autoconversion of cloud water to rain. *.true.* by default.

z_slope_ice

Logical: Set *.true.* to turn on vertically subgrid linear monotonic slope for autoconversion of cloud ice to snow. *.true.* by default.

C.4   Fall Speed

const_vi

Logical: Set *.true.* to use constant cloud ice terminal fall velocity. *.false.* by default.

const_vs

Logical: Set *.true.* to use constant snow terminal fall velocity. *.false.* by default.

const_vg

Logical: Set *.true.* to use constant graupel terminal fall velocity. *.false.* by default.

const_vr

Logical: Set *.true.* to use constant rain terminal fall velocity. *.false.* by default.

vi_fac

Real: Scale factor for cloud ice fall or the constant cloud ice terminal fall velocity when **const_vi** is *.true.*. The unit is 1. 1 by default.

vr_fac

Real: Scale factor for rain fall or the constant rain terminal fall velocity when **const_vr** is *.true.*. The unit is 1. 1 by default.

vs_fac

Real: Scale factor for snow fall or the constant snow terminal fall velocity when **const_vs** is *.true.*. The unit is 1. 1 by default.

vg_fac

Real: Scale factor for graupel fall or the constant graupel terminal fall velocity when **const_vg** is *.true.*. The unit is 1. 1 by default.

vi_max

Real: Maximum terminal fall velocity for cloud ice. The unit is ms^{-1}. 1 as default.

vs_max

Real: Maximum terminal fall velocity for snow. The unit is ms^{-1}. 2 as default.

vg_max

Real: Maximum terminal fall velocity for graupel. The unit is ms^{-1}. 12 as default.

vr_max

Real: Maximum terminal fall velocity for rain. The unit is ms^{-1}. 12 as default.

C.5 Conversion Threshold

ql_mlt

Real: Maximum value of cloud water allowed from melted cloud ice (cloud ice $\rightarrow$ cloud water or rain). Exceed of which will become rain. Increasing / decreasing **ql_mlt** can increase / decrease cloud water and decrease / increase rain. The unit is $kgkg^{-1}$. 1.0×10^{-3} by default.

qs_mlt

Real: Maximum value of cloud water allowed from melted snow (snow $\rightarrow$ cloud water or rain). Exceed of which will become rain. Increasing / decreasing **qs_mlt** can increase / decrease cloud water and decrease / increase rain. The unit is $kgkg^{-1}$. 1.0×10^{-6} by default.

ql_gen

Real: Maximum value for cloud water generated from condensation of water vapor (water vapor $\rightarrow$ cloud water). Increasing / decreasing **ql_gen** can increase / decrease cloud water. The unit is $kgkg^{-1}$. 1.0×10^{-3} by default.

ql0_max

Real: Threshold of cloud water to rain autoconversion (cloud water $\rightarrow$ rain). Increasing / decreasing **ql0_max** can increase / decrease cloud water and decrease / increase rain. The unit is $kgkg^{-1}$. 2.0×10^{-3} by default.

qi0_max

Real: Maximum value of cloud ice generated from other sources like convection. Exceed of which will become snow. Increasing / decreasing **qi0_max** can increase / decrease cloud ice and decrease / increase snow. The unit is $kgkg^{-1}$. 1.0×10^{-4} by default.

qi0_crt

Real: Threshold of cloud ice to snow autoconversion (cloud ice $\rightarrow$ snow). Increasing / decreasing **qi0_crt** can increase / decrease cloud ice and decrease / increase snow. The unit is kgm^{-3}. 8×10^{-5} by default.

qs0_crt

Real: Threshold of snow to graupel autoconversion (snow $\rightarrow$ graupel). Increasing / decreasing **qs0_crt** can increase / decrease snow and decrease / increase graupel. The unit is kgm^{-3}. 1.0×10^{-3} by default.

qi_lim

Real: Cloud ice limiter to prevent ice built up in cloud ice freezing (cloud water $\rightarrow$ cloud ice) and deposition (water vapor $\rightarrow$ cloud ice). The unit is 1. 1 by default.

rh_inc

Real: Relative humidity increment for complete evaporation of cloud water and cloud ice. The unit is 1. 0.3 by default.

rh_ins

Real: Relative humidity increment for minimum evaporation of rain. The unit is 1. 0.3 by default.

rh_inr

Real: Relative humidity increment for rain evaporation. The unit is 1. 0.3 by default.

rthresh

Real: Critical cloud water radius for autoconversion (cloud water $\rightarrow$ rain). Increasing / decreasing of **rthresh** can slow down / speed up the autoconversion. The unit is mm. 1.0×10^{-5} by default.

C.6 Conversion Efficiency

c_pracw

Real: Accretion efficiency of cloud water to rain (cloud water $\rightarrow$ rain). Increasing / decreasing of

c_pracw can speed up / slow down the accretion of cloud water by rain. The unit is 1. 0.9 by default.

c_psacw

Real: Accretion efficiency of cloud water to snow (cloud water → snow). Increasing / decreasing of **c_psacw** can speed up / slow down the accretion of cloud water by snow. The unit is 1. 1 by default.

c_pgacw

Real: Accretion efficiency of cloud water to graupel (cloud water → graupel). Increasing / decreasing of **c_pgacw** can speed up / slow down the accretion of cloud water by graupel. The unit is 1. 1 by default.

c_psaci

Real: Accretion efficiency of cloud ice to snow (cloud ice → snow). Increasing / decreasing of **c_psaci** can speed up / slow down the accretion of cloud ice by snow. The unit is 1. 0.02 by default.

c_pgaci

Real: Accretion efficiency of cloud ice to graupel (cloud ice → graupel). Increasing / decreasing of **c_pgaci** can speed up / slow down the accretion of cloud ice by graupel. The unit is 1. 0.05 by default.

c_praci

Real: Accretion efficiency of cloud ice to rain (cloud ice → rain). Increasing / decreasing of **c_praci** can speed up / slow down the accretion of cloud ice by rain. The unit is 1. 1 by default.

c_pgacs

Real: Accretion efficiency of snow to graupel (snow → graupel). Increasing / decreasing of **c_pgacs** can speed up / slow down the accretion of snow by graupel. The unit is 1. 0.01 by default.

c_pracs

Real: Accretion efficiency of snow to rain (snow → rain). Increasing / decreasing of **c_pracs** can speed up / slow down the accretion of snow by rain. The unit is 1. 1 by default.

c_psacr

Real: Accretion efficiency of rain to snow (rain → snow). Increasing / decreasing of **c_psacr** can speed up / slow down the accretion of rain by snow. The unit is 1. 1 by default.

c_pgacr

Real: Accretion efficiency of rain to graupel (rain → graupel). Increasing / decreasing of **c_pgacr** can speed up / slow down the accretion of rain by graupel. The unit is 1. 1 by default.

c_paut

Real: Autoconversion efficiency of cloud water to rain (cloud water → rain). Increasing / decreasing of **c_paut** can speed up / slow down the autoconversion of cloud water to rain. The unit is 1. 0.5 by default.

C.7 Options

cfflag

Cloud fraction scheme. 1: GFDL cloud scheme; 2: Xu and Randall (1996); 3: Park et al. (2016); 4: Gultepe and Isaac (2007). 1 by default.

icloud_f

GFDL cloud scheme. 0: subgrid variability based scheme; 1: same as 0, but for old fvgfs implementation; 2: binary cloud scheme; 3: extension of 0. 0 by default.

irain_f

Cloud water to rain auto conversion scheme. 0: subgrid variability based scheme; 1: no subgrid varaibility. 0 by default.

inflag

Ice nucleation scheme. 1: Hong et al. (2004); 2: Meyers et al. (1992); 3: Meyers et al. (1992); 4: Cooper (1986); 5: Fletcher et al. (1962). 1 by default.

igflag

Ice generation scheme. 1: WSM6; 2: WSM6 with 0 at 0 C; 3: WSM6 with 0 at 0 C and fixed value at - 10 C; 4: combination of 1 and 3. 3 by default.

ifflag

Ice fall scheme. 1: Deng and Mace (2008); 2: Heymsfield and Donner (1990). 1 by default.

rewflag

Cloud water effective radius scheme. 1: Martin et al. (1994); 2: Martin et al. (1994), GFDL revision; 3: Kiehl (1994). 1 by default.

reiflag

Cloud water effective radius scheme. 1: Heymsfield and McFarquhar (1996); 2: Donner et al. (1997); 3: Fu (2007); 4: Kristjansson et al. (2000); 5: Wyser (1998); 6: Sun and Rikus (1999); Sun (2001). 5 by default.

rerflag

Rain effective radius scheme. 1: effective radius; 2: mass-weighted effective radius. 1 by default.

resflag

Snow effective radius scheme. 1: effective radius; 2: mass-weighted effective radius. 1 by default.

regflag

Graupel effective radius scheme. 1: effective radius; 2: mass-weighted effective radius. 1 by default.

radr_flag

Radar reflectivity for rain. 1: Stoelinga (2005); 2: Smith et al. (1975); Tong and Xue (2005); 3: Marshall-Palmer formula (https://en.wikipedia.org/wiki/DBZ_(meteorology)). 1 by default.

rads_flag

Radar reflectivity for snow. 1: Stoelinga (2005); 2: Smith et al. (1975); Tong and Xue (2005); 3: Marshall-Palmer formula (https://en.wikipedia.org/wiki/DBZ_(meteorology)). 1 by default.

radg_flag

Radar reflectivity for graupel. 1: Stoelinga (2005); 2: Smith et al. (1975); Tong and Xue (2005); 3: Marshall-Palmer formula (https://en.wikipedia.org/wiki/DBZ_(meteorology)). 1 by default.

do_hail

Logical: Set .*true*. to change all graupel properties to hail properties so that graupel becomes hail. .*false*. by default.

do_cond_timescale

Logical: Set .*true*. to scale cloud water condensation to make it slower. .*false*. by default.

use_rhc_cevap

Logical: Set .*true*. to reduce evaporation / condensation by adding a cap. .*false*. by default.

use_rhc_revap

Logical: Set .*true*. to reduce evaporation / condensation by adding a relative humidity threshold. .*false*. by default.

liq_ice_combine

Logical: Set .*true*. to combine all liquid water, combine all solid water in cloud effective radius diagnostic. .*false*. by default.

snow_grauple_combine

Logical: Set .*true*. to combine snow and graupel in cloud effective radius diagnostic. .*true*. by default.

do_warm_rain_mp

> Logical: Set *.true.* to do warm rain microphysics only. It removes all ice microphysics processes. *.false.* by default.

C.8   Cloud Fraction

do_qa

> Logical: Set *.true.* to activate cloud fraction diagnosis. *.true.* as default.

rad_rain

> Logical: Set *.true.* to consider rain in cloud fraction calculation. *.true.* by default.

rad_snow

> Logical: Set *.true.* to consider snow in cloud fraction calculation. *.true.* by default.

rad_graupel

> Logical: Set *.true.* to consider graupel in cloud fraction calculation. *.true.* by default.

do_cld_adj

> Logical: Set *.true.* to adjust cloud fraction based on the Xu and Randall (1996) scheme. *.false.* by default.

cld_min

> Real: Minimum cloud fraction. If total cloud condensate exceeds $1 \times 10^{-6} kgkg^{-1}$, cloud fraction cannot be less than **cld_min**. The unit is 1. 0.05 by default.

xr_a

> Real: p value in Xu and Randall (1996). 0.25 by default.

xr_b

> Real: alpha_0 value in Xu and Randall (1996). 100 by default.

xr_c

> Real: gamma value in Xu and Randall (1996). 0.49 by default.

C.9   Sedimentation

use_ppm

> Logical: Set *.true.* to use PPM fall scheme. *.false.* to use time-implicit monotonic fall scheme. *.false.* by default.

mono_prof

> Logical: Set *.true.* to turn on terminal fall with monotonic PPM scheme. This is used together with **use_ppm** = *.true.*. *.true.* by default.

do_sedi_uv

> Logical: Set *.true.* to turn on horizontal momentum transport during sedimentation. *.true.* by default.

do_sedi_w

> Logical: Set *.true.* to turn on vertical motion transport during sedimentation. *.true.* by default.

do_sedi_heat

> Logical: Set *.true.* to turn on heat transport during sedimentation. *.true.* by default.

do_sedi_melt

> Logical: Set *.true.* to turn on cloud ice, snow, and graupel melting during sedimentation. *.true.* by default.

C.10 CCN

prog_ccn

 Logical: Set *.true.* to activate prognostic CCN. *.false.* by default.

ccn_l

 Real: Base CCN over land. Increasing / decreasing **ccn_l** can slow down / speed up the autoconversion of cloud water to rain (cloud water $\rightarrow$ rain). The unit is cm^{-3}. 270 by default.

ccn_o

 Real: Base CCN over ocean. Increasing / decreasing **ccn_o** can slow down / speed up the autoconversion of cloud water to rain (cloud water $\rightarrow$ rain). The unit is cm^{-3}. 90 by default.

C.11 Others

tice_mlt

 Real: Melting temperature. The unit is K. 273.16 by default.

alin

 Real: Parameter a in Lin et al. (1983). Constant in empirical formula for U_R. Increasing / decreasing **alin** can boost / decrease accretion of cloud water by rain (cloud water $\rightarrow$ rain) and rain evaporation (rain $\rightarrow$ water vapor). The unit is $cm^{1-b}s^{-1}$. 842 by default. This value follows Hong and Lim (2006).

blin

 Real: Parameter b in Lin et al. (1983).The unit is 1. 0.8 by default.

clin

 Real: Parameter c in Lin et al. (1983). Constant in empirical formula for U_S. Increase / decreasing **clin** can boost / decrease accretion of cloud water by snow (cloud water $\rightarrow$ snow), accretion of cloud ice by snow (cloud ice $\rightarrow$ snow), snow sublimation and deposition (snow $\leftrightarrow$ water vapor), and snow melting (snow $\rightarrow$ cloud water or rain). The unit is $cm^{1-d}s^{-1}$. 4.8 by default.

dlin

 Real: Parameter d in Lin et al. (1983).The unit is 1. 0.25 by default.

elin

 Real: Parameter e in Lin et al. (1983). Constant in empirical formula for U_G. Increase / decreasing **elin** can boost / decrease accretion of cloud water by graupel (cloud water $\rightarrow$ graupel), accretion of cloud ice by graupel (cloud ice $\rightarrow$ graupel), graupel sublimation and deposition (graupel $\leftrightarrow$ water vapor), and graupel melting (graupel $\rightarrow$ cloud water or rain). The unit is $cm^{1-d}s^{-1}$. 1 by default.

flin

 Real: Parameter f in Lin et al. (1983).The unit is 1. 0.5 by default.

t_min

 Real: Temperature threshold for instant deposition. Deposit all water vapor to cloud ice (water vapor $\rightarrow$ cloud ice) when temperature is lower than **t_min**. The unit is K. 178 by default.

t_sub

 Real: Temperature threshold for sublimation. Cloud ice, snow or graupel stops / starts sublimation (cloud ice $\rightarrow$ water vapor, snow $\rightarrow$ water vapor, graupel $\rightarrow$ water vapor) when temperature is lower / higher than **t_sub**. The unit is K. 184 by default.

te_err

 Real: Use in total energy and total water checker. 64bit: 1×10^{-14}, 32bit: 1×10^{-7}; turn off to save computer time. 1×10^{-14} by default.

Appendix D   Document Update Record

- 2022.07.01 Document version 4.0: Used GFDL MP as a short name for "GFDL single-moment five-category cloud microphysics scheme". Clarify the 3rd latent heat coefficient, horizontal subgrid variability, particle size distribution, cloud fraction and radar reflectivity, and cloud drop number concentration. Made some corrections to the saturated specific humidity. Updated GitHub information. Updated the features subsection. Cleaned up the microphysical processes section. Removed unused figures.

- 2021.10.09 Document version 3.1: some updates to the introduction section.

- 2021.02.16 Document version 3.0: the whole document was overwritten because the whole code was overwritten.

- 2019.10.30 Document version 2.3: title changed, more references were included, revised many places to correctly represent the size distribution, and mentioned the plan to develop the double-moment scheme.

- 2019.10.14 Document version 2.2: minor update to the number concentration of cloud ice.

- 2019.09.06 Document version 2.1: added a reference to cloud fraction scheme I, updated basic equations, removed some red text that has been implemented into the code, updated some formulas, updated the List of Symbols.

- 2019.08.28 Document version 2.0: revised the whole document based on the latest version of the GFDL MP.

- 2017.10.16 Document version 1.1: updated authors' affiliations, corrected snow melting equation in fast saturation adjustment, added namelist guide.

- 2017.07.25 Document version 1.0: adjusted the line spacing, updated author list.

- 2017.07.22 Document version 0.7: updated figure 2, updated appendix A and B, revised the CNN formula, added Figure 3,5,6. The whole document has been revised.

- 2017.06.02 Document version 0.6: added distribution declaration, cleaned up main text and formulas, enriched the description of the formulas and included their source and derivation method, fixed some errors, revised the appendix tables, updated the constants and tuning parameters, updated figure 1

- 2017.01.31 Document version 0.5: updated some parameters (according to gfdl_mp_dev branch), fixed some errors in the formulas and units, added the comparison to IFS constants.

- 2016.11.17 Document version 0.4: revised according to code change (according to gfdl_mp branch), completed radius diagnosis.

- 2016.11.04 Document version 0.3: revised the title page, added the references of formulas, corrected several errors, added a new section called reflectivity diagnosis, a new section called Lagrangian falls of hydrometeors.

- 2016.10.28 Document version 0.2: added contents, source / sink flow chart, references, basic equations, unified the name of source / sink terms, added a new section called interaction with convection and radiation, a new appendix section called some cloud microphysics parameters, acknowledgment, revised the whole document, corrected the errors, those are not consistent with the code are marked as red color.

- 2016.10.20 Document version 0.1: first draft, mainly listing all equations / processes in the GFDL cloud microphysics scheme.

- 2016.10.14 Document version 0.0: initiated this document.

Acknowledgement

Code, Copyright, and Citation

The source code of this document is available on GitHub (https://github.com/linjiongzhou/GFDL-MP). The source code of the GFDL MP is also available on GitHub in the FV3 repository (https://github.com/NOAA-GFDL/GFDL_atmos_cubed_sphere/).

References

Arnold, N. P., W. M. Putman, and S. R. Freitas, 2020: Impact of resolution and parameterized convection on the diurnal cycle of precipitation in a global nonhydrostatic model. *Journal of the Meteorological Society of Japan. Ser. II*, **98 (6)**, 1279–1304, doi:https://doi.org/10.2151/jmsj.2020-066.

Baba, Y., and K. Takahashi, 2014: Dependency of stratiform precipitation on a two-moment cloud microphysical scheme in mid-latitude squall line. *Atmospheric Research*, **138**, 394–413, doi:https://doi.org/10.1016/j.atmosres.2013.12.009.

Baldauf, M., A. Seifert, J. Forstner, D. Majewski, M. Raschendorfer, and T. Reinhardt, 2011: Operational convective-scale numerical weather prediction with the cosmo model: Description and sensitivities. *Monthly Weather Review*, **139 (12)**, 3887–3905, doi:https://doi.org/10.1175/Mwr-D-10-05013.1.

Bauer, P., A. Thorpe, and G. Brunet, 2015: The quiet revolution of numerical weather prediction. *Nature*, **525 (7567)**, 47–55, doi:https://doi.org/10.1038/nature14956.

Bigg, E. K., 1953: The supercooling of water. *Proceedings of the Physical Society of London Section B*, **66 (404)**, 688–694, doi:https://doi.org/10.1088/0370-1301/66/8/309.

Boucher, O., and U. Lohmann, 1995: The sulfate-ccn-cloud albedo effect. *Tellus B*, **47 (3)**, 281–300, doi:https://doi.org/10.1034/j.1600-0889.47.issue3.1.x.

Chen, J.-H., and S.-J. Lin, 2011: The remarkable predictability of inter-annual variability of atlantic hurricanes during the past decade. *Geophysical Research Letters*, **38 (11)**, L11 804, doi:https://doi.org/10.1029/2011GL047629.

Chen, J. H., and S. J. Lin, 2013: Seasonal predictions of tropical cyclones using a 25-km-resolution general circulation model. *Journal of Climate*, **26 (2)**, 380–398, doi:https://doi.org/10.1175/Jcli-D-12-00061.1.

Chen, J.-H., S.-J. Lin, L. Zhou, X. Chen, S. Rees, M. Bender, and M. Morin, 2019a: Evaluation of tropical cyclone forecasts in the next generation global prediction system. *Monthly Weather Review*, **147 (9)**, 3409–3428, doi:https://doi.org/10.1175/MWR-D-18-0227.1.

Chen, J.-H., and Coauthors, 2019b: Advancements in hurricane prediction with noaa's next-generation forecast system. *Geophysical Research Letters*, **46 (8)**, 4495–4501, doi:https://doi.org/10.1029/2019GL082410.

Cooper, W. A., 1986: *Ice Initiation in Natural Clouds*, book section Chapter 4, 29–32. American Meteorological Society, Boston, MA, doi:https://doi.org/10.1007/978-1-935704-17-1_4.

Cotton, W. R., G. J. Tripoli, R. M. Rauber, and E. A. Mulvihill, 1986: Numerical-simulation of the effects of varying ice crystal nucleation rates and aggregation processes on orographic snowfall. *Journal of Climate and Applied Meteorology*, **25 (11)**, 1658–1680, doi:https://doi.org/10.1175/1520-0450(1986)025⟨1658:Nsoteo⟩2.0.Co;2.

Dawson, D. T., M. Xue, J. A. Milbrandt, and M. K. Yau, 2010: Comparison of evaporation and cold pool development between single-moment and multimoment bulk microphysics schemes in idealized simulations of tornadic thunderstorms. *Monthly Weather Review*, **138 (4)**, 1152–1171, doi:https://doi.org/10.1175/2009mwr2956.1.

Deng, M., and G. G. Mace, 2008: Cirrus cloud microphysical properties and air motion statistics using cloud radar doppler moments: Water content, particle size, and sedimentation relationships. *Geophysical Research Letters*, **35 (17)**, L17808, doi:https://doi.org/10.1029/2008gl035054.

Dong, J., and Coauthors, 2020: The evaluation of real-time hurricane analysis and forecast system (hafs) stand-alone regional (sar) model performance for the 2019 atlantic hurricane season. *Atmosphere*, **11 (617)**, 1–16, doi:https://doi.org/10.3390/atmos11060617.

Donner, L. J., C. J. Seman, B. J. Soden, R. S. Hemler, J. C. Warren, J. Strom, and K. N. Liou, 1997: Large-scale ice clouds in the gfdl skyhi general circulation model. *Journal of Geophysical Research-Atmospheres*, **102 (D18)**, 21745–21768, doi:https://doi.org/10.1029/97jd01488.

Dudhia, J., 1989: Numerical study of convection observed during the winter monsoon experiment using a mesoscale two-dimensional model. *Journal of the Atmospheric Sciences*, **46 (20)**, 3077–3107, doi:https://doi.org/10.1175/1520-0469(1989)046⟨3077:Nsocod⟩2.0.Co;2.

Emanuel, K. A., 1994: *Atmospheric convection*. Oxford University Press, New York, x, 580 p. pp.

Fletcher, N. H., P. Squires, and E. G. Bowen, 1962: *The Physics of Rainclouds*. University Press, New York, 386 p. pp.

Fu, Q., 2007: A new parameterization of an asymmetry factor of cirrus clouds for climate models. *Journal of the Atmospheric Sciences*, **64 (11)**, 4140–4150, doi:https://doi.org/10.1175/2007jas2289.1.

Gao, K., J.-H. Chen, L. M. Harris, S.-J. Lin, B. Xiang, and M. Zhao, 2017: Impact of intraseasonal oscillations on the tropical cyclone activity over the gulf of mexico and western caribbean sea in gfdl hiram. *Journal of Geophysical Research: Atmospheres*, **122 (24)**, 13,125–13,137, doi:https://doi.org/10.1002/2017JD027756.

Gao, K., L. Harris, J.-H. Chen, S.-J. Lin, and A. Hazelton, 2019: Improving agcm hurricane structure with two-way nesting. *Journal of Advances in Modeling Earth Systems*, **11 (1)**, 278–292, doi:https://doi.org/10.1029/2018MS001359.

Gultepe, I., and G. A. Isaac, 2007: Cloud fraction parameterization as a function of mean cloud water content and its variance using in-situ observations. *Geophysical Research Letters*, **34 (7)**, L07801, doi:https://doi.org/10.1029/2006gl028223.

Harris, L., X. Chen, W. Putman, L. Zhou, and J. Chen, 2021: A scientifc description of the gfdl finite-volume cubed-sphere dynamical core. Tech. rep. doi:https://doi.org/10.25923/6nhs-5897, URL https://repository.library.noaa.gov/view/noaa/30725.

REFERENCES

Harris, L., and Coauthors, 2020: Gfdl shield: A unified system for weather-to-seasonal prediction. *Journal of Advances in Modeling Earth Systems*, **12 (10)**, e2020MS002 223, doi:https://doi.org/10.1029/2020ms002223.

Harris, L. M., S. J. Lin, and C. Y. Tu, 2016: High-resolution climate simulations using gfdl hiram with a stretched global grid. *Journal of Climate*, **29 (11)**, 4293–4314, doi:https://doi.org/10.1175/Jcli-D-15-0389.1.

Harris, L. M., S. L. Rees, M. Morin, L. Zhou, and W. F. Stern, 2019: Explicit prediction of continental convection in a skillful variable-resolution global model. *Journal of Advances in Modeling Earth Systems*, **11 (6)**, 1847–1869, doi:https://doi.org/10.1029/2018MS001542.

Hazelton, A., G. J. Alaka, L. Cowan, M. Fischer, and S. Gopalakrishnan, 2021: Understanding the processes causing the early intensification of hurricane dorian through an ensemble of the hurricane analysis and forecast system (hafs). *Atmosphere*, **12 (93)**, 2–26, doi:https://doi.org/10.3390/atmos12010093.

He, B., and Coauthors, 2019: Cas fgoals-f3-l model datasets for cmip6 historical atmospheric model intercomparison project simulation. *Advances in Atmospheric Sciences*, **36 (8)**, 771–778, doi:https://doi.org/10.1007/s00376-019-9027-8.

Heymsfield, A. J., and L. J. Donner, 1990: A scheme for parameterizing ice-cloud water-content in general-circulation models. *Journal of the Atmospheric Sciences*, **47 (15)**, 1865–1877, doi:https://doi.org/10.1175/1520-0469(1990)047⟨1865:Asfpic⟩2.0.Co;2.

Heymsfield, A. J., and G. M. McFarquhar, 1996: High albedos of cirrus in the tropical pacific warm pool: Microphysical interpretations from cepex and from kwajalein, marshall islands. *Journal of the Atmospheric Sciences*, **53 (17)**, 2424–2451, doi:https://doi.org/10.1175/1520-0469(1996)053⟨2424:Haocit⟩2.0.Co;2.

Hong, S. Y., J. Dudhia, and S. H. Chen, 2004: A revised approach to ice microphysical processes for the bulk parameterization of clouds and precipitation. *Monthly Weather Review*, **132 (1)**, 103–120, doi:https://doi.org/10.1175/1520-0493(2004)132⟨0103:Aratim⟩2.0.Co;2.

Hong, S. Y., and J. O. J. Lim, 2006: The wrf single-moment 6-class microphysics scheme (wsm6). *Asia-Pacific Journal of Atmospheric Sciences*, **42 (2)**, 129–151, URL http://www.dbpia.co.kr/Article/NODE00937254.

Houze, R. A., 2014: *Cloud dynamics*. Second edition. ed., Academic Press is an imprint of Elsevier, Amsterdam ; New York, xxiii, 432 pages pp.

Igel, A. L., M. R. Igel, and S. C. van den Heever, 2015: Make it a double? sobering results from simulations using single-moment microphysics schemes. *Journal of the Atmospheric Sciences*, **72 (2)**, 910–925, doi:https://doi.org/10.1175/jas-d-14-0107.1.

Jakob, C., and S. A. Klein, 2000: A parametrization of the effects of cloud and precipitation overlap for use in general-circulation models. *Quarterly Journal of the Royal Meteorological Society*, **126 (568)**, 2525–2544, doi:https://doi.org/10.1256/smsqj.56808.

Jeevanjee, N., 2017: Vertical velocity in the gray zone. *Journal of Advances in Modeling Earth Systems*, **9 (6)**, 2304–2316, doi:https://doi.org/10.1002/2017ms001059.

Jeevanjee, N., and L. Zhou, 2022: On the resolution-dependence of anvil cloud fraction and precipitation efficiency in radiative-convective equilibrium. *Journal of Advances in Modeling Earth Systems*, **14 (3)**, e2021MS002 759, doi:https://doi.org/10.1029/2021ms002759.

Jin, Y., and Coauthors, 2014: The impact of ice phase cloud parameterizations on tropical cyclone prediction. *Monthly Weather Review*, **142 (2)**, 606–625, doi:https://doi.org/10.1175/mwr-d-13-00058.1.

Jung, Y. S., M. Xue, and M. J. Tong, 2012: Ensemble kalman filter analyses of the 29-30 may 2004 oklahoma tornadic thunderstorm using one- and two-moment bulk microphysics schemes, with verification against polarimetric radar data. *Monthly Weather Review*, **140 (5)**, 1457–1475, doi:https://doi.org/10.1175/Mwr-D-11-00032.1.

Khain, A. P., and M. Pinsky, 2018: *Physical Processes in Clouds and Cloud Modeling*. Cambridge University Press, Cambridge, doi:https://doi.org/10.1017/9781139049481.

Kiehl, J. T., 1994: Sensitivity of a gcm climate simulation to differences in continental versus maritime cloud drop size. *Journal of Geophysical Research-Atmospheres*, **99 (D11)**, 23 107–23 115, doi:https://doi.org/10.1029/94jd01117.

Klein, S. A., and C. Jakob, 1999: Validation and sensitivities of frontal clouds simulated by the ecmwf model. *Monthly Weather Review*, **127 (10)**, 2514–2531, doi:https://doi.org/10.1175/1520-0493(1999)127⟨2514:Vasofc⟩2.0.Co;2.

Knutson, T. R., J. J. Sirutis, S. T. Garner, I. M. Held, and R. E. Tuleya, 2007: Simulation of the recent multidecadal increase of atlantic hurricane activity using an 18-km-grid regional model. *Bulletin of the American Meteorological Society*, **88 (10)**, 1549–1565, doi:https://doi.org/10.1175/Bams-88-10-1549.

Knutson, T. R., J. J. Sirutis, S. T. Garner, G. A. Vecchi, and I. M. Held, 2008: Simulated reduction in atlantic hurricane frequency under twenty-first-century warming conditions. *Nature Geosci*, **1 (6)**, 359–364, doi:https://doi.org/10.1038/ngeo202.

Kogan, Y., 2013: A cumulus cloud microphysics parameterization for cloud-resolving models. *Journal of the Atmospheric Sciences*, **70 (5)**, 1423–1436, doi:https://doi.org/10.1175/Jas-D-12-0183.1.

Kristjansson, J. E., J. M. Edwards, and D. L. Mitchell, 2000: Impact of a new scheme for optical properties of ice crystals on climates of two gcms. *Journal of Geophysical Research: Atmospheres*, **105 (D8)**, 10 063–10 079, doi:https://doi.org/10.1029/2000jd900015.

Krueger, S. K., Q. A. Fu, K. N. Liou, and H. N. S. Chin, 1995: Improvements of an ice-phase microphysics parameterization for use in numerical simulations of tropical convection. *Journal of Applied Meteorology*, **34 (1)**, 281–287, doi:https://doi.org/10.1175/1520-0450-34.1.281.

Lamb, D., and J. Verlinde, 2011: *Physics and chemistry of clouds*. Cambridge University Press, Cambridge ; New York, xiv, 584 p. pp.

Le Trent, H., and Z.-X. Li, 1991: Sensitivity of an atmospheric general circulation model to prescribed sst changes: feedback effects associated with the simulation of cloud optical properties. *Climate Dynamics*, **5 (3)**, 175–187, doi:https://doi.org/10.1007/bf00251808.

Li, J., Q. Bao, Y. Liu, G. Wu, L. Wang, B. He, X. Wang, and J. Li, 2019: Evaluation of famil2 in simulating the climatology and seasonal-to-interannual variability of tropical cyclone characteristics. *Journal of Advances in Modeling Earth Systems*, **11 (4)**, 1117–1136, doi:https://doi.org/10.1029/2018ms001506.

Lin, S.-J., 2004: A "vertically lagrangian" finite-volume dynamical core for global models. *Monthly Weather Review*, **132 (10)**, 2293–2307, doi:https://doi.org/10.1175/1520-0493(2004)132⟨2293:Avlfdc⟩2.0.Co;2.

Lin, S.-J., W. C. Chao, Y. C. Sud, and G. K. Walker, 1994: A class of the van leer-type transport schemes and its application to the moisture transport in a general circulation model. *Monthly Weather Review*, **122 (7)**, 1575–1593, doi:https://doi.org/10.1175/1520-0493(1994)122⟨1575:Acotvl⟩2.0.Co;2.

Lin, Y. L., R. D. Farley, and H. D. Orville, 1983: Bulk parameterization of the snow field in a cloud model. *Journal of Climate and Applied Meteorology*, **22 (6)**, 1065–1092, doi:https://doi.org/10.1175/1520-0450(1983)022⟨1065:Bpotsf⟩2.0.Co;2.

Lord, S. J., H. E. Willoughby, and J. M. Piotrowicz, 1984: Role of a parameterized ice-phase microphysics in an axisymmetric, nonhydrostatic tropical cyclone model. *Journal of the Atmospheric Sciences*, **41 (19)**, 2836–2848, doi:https://doi.org/10.1175/1520-0469(1984)041⟨2836:Roapip⟩2.0.Co;2.

Luo, Y. L., K. M. Xu, H. Morrison, and G. McFarquhar, 2008: Arctic mixed-phase clouds simulated by a cloud-resolving model: Comparison with arm observations and sensitivity to microphysics parameterizations. *Journal of the Atmospheric Sciences*, **65 (4)**, 1285–1303, doi:https://doi.org/10.1175/2007jas2467.1.

Martin, G. M., D. W. Johnson, and A. Spice, 1994: The measurement and parameterization of effective radius of droplets in warm stratocumulus clouds. *Journal of the Atmospheric Sciences*, **51 (13)**, 1823–1842, doi:https://doi.org/10.1175/1520-0469(1994)051⟨1823:Tmapoe⟩2.0.Co;2.

Meyers, M. P., P. J. DeMott, and W. R. Cotton, 1992: New primary ice-nucleation parameterizations in an explicit cloud model. *Journal of Applied Meteorology*, **31 (7)**, 708–721, doi:https://doi.org/10.1175/1520-0450(1992)031⟨0708:Npinpi⟩2.0.Co;2.

Milbrandt, J. A., and R. McTaggart-Cowan, 2010: Sedimentation-induced errors in bulk microphysics schemes. *Journal of the Atmospheric Sciences*, **67 (12)**, 3931–3948, doi:https://doi.org/10.1175/2010jas3541.1.

Molthan, A. L., and B. A. Colle, 2012: Comparisons of single- and double-moment microphysics schemes in the simulation of a synoptic-scale snowfall event. *Monthly Weather Review*, **140 (9)**, 2982–3002, doi:https://doi.org/10.1175/Mwr-D-11-00292.1.

Moore, E. B., and V. Molinero, 2011: Structural transformation in supercooled water controls the crystallization rate of ice. *Nature*, **479 (7374)**, 506–8, doi:https://doi.org/10.1038/nature10586.

Morrison, H., and W. W. Grabowski, 2008: A novel approach for representing ice microphysics in models: Description and tests using a kinematic framework. *Journal of the Atmospheric Sciences*, **65 (5)**, 1528–1548, doi:https://doi.org/10.1175/2007jas2491.1.

Morrison, H., G. Thompson, and V. Tatarskii, 2009: Impact of cloud microphysics on the development of trailing stratiform precipitation in a simulated squall line: Comparison of one- and two-moment schemes. *Monthly Weather Review*, **137 (3)**, 991–1007, doi:https://doi.org/10.1175/2008mwr2556.1.

Nogherotto, R., A. M. Tompkins, G. Giuliani, E. Coppola, and F. Giorgi, 2016: Numerical framework and performance of the new multiple-phase cloud microphysics scheme in regcm4.5: precipitation, cloud microphysics, and cloud radiative effects. *Geoscientific Model Development*, **9 (7)**, 2533–2547, doi:https://doi.org/10.5194/gmd-9-2533-2016.

Park, R. S., J. H. Chae, and S. Y. Hong, 2016: A revised prognostic cloud fraction scheme in a global forecasting system. *Monthly Weather Review*, **144 (3)**, 1219–1229, doi:https://doi.org/10.1175/Mwr-D-15-0273.1.

Pauluis, O., and S. Garner, 2006: Sensitivity of radiative-convective equilibrium simulations to horizontal resolution. *Journal of the Atmospheric Sciences*, **63 (7)**, 1910–1923, doi:https://doi.org/10.1175/Jas3705.1.

Pruppacher, H. R., and J. D. Klett, 2010: *Microphysics of Clouds and Precipitation*. 2nd ed., Atmospheric and Oceanographic Sciences Library, Springer Netherlands, XXII, 954 pp., doi:https://doi.org/10.1007/978-0-306-48100-0.

Reisner, J., R. M. Rasmussen, and R. T. Bruintjes, 1998: Explicit forecasting of supercooled liquid water in winter storms using the mm5 mesoscale model. *Quarterly Journal of the Royal Meteorological Society*, **124 (548)**, 1071–1107, doi:https://doi.org/10.1002/qj.49712454804.

Rogers, R. R., and M. K. Yau, 1989: *S Short Course in Cloud Physics*. Third edition ed., Butterworth and Heinemann, Oxford.

Rotstayn, L. D., 1997: A physically based scheme for the treatment of stratiform clouds and precipitation in large-scale models. i: Description and evaluation of the microphysical processes. *Quarterly Journal of the Royal Meteorological Society*, **123 (541)**, 1227–1282, doi:https://doi.org/10.1002/qj.49712354106.

Rotstayn, L. D., B. F. Ryan, and J. J. Katzfey, 2000: A scheme for calculation of the liquid fraction in mixed-phase stratiform clouds in large-scale models. *Monthly Weather Review*, **128 (4)**, 1070–1088, doi:https://doi.org/10.1175/1520-0493(2000)128⟨1070:Asfcot⟩2.0.Co;2.

Rutledge, S. A., and P. Hobbs, 1983: The mesoscale and microscale structure and organization of clouds and precipitation in midlatitude cyclones. viii: A model for the "seeder-feeder" process in warm-frontal rainbands. *Journal of the Atmospheric Sciences*, **40 (5)**, 1185–1206, doi:https://doi.org/10.1175/1520-0469(1983)040⟨1185:Tmamsa⟩2.0.Co;2.

Rutledge, S. A., and P. V. Hobbs, 1984: The mesoscale and microscale structure and organization of clouds and precipitation in midlatitude cyclones. xii: A diagnostic modeling study of precipitation development in narrow cold-frontal rainbands. *Journal of the Atmospheric Sciences*, **41 (20)**, 2949–2972, doi:https://doi.org/10.1175/1520-0469(1984)041⟨2949:Tmamsa⟩2.0.Co;2.

Satoh, M., T. Matsuno, H. Tomita, H. Miura, T. Nasuno, and S. Iga, 2008: Nonhydrostatic icosahedral atmospheric model (nicam) for global cloud resolving simulations. *Journal of Computational Physics*, **227 (7)**, 3486–3514, doi:https://doi.org/10.1016/j.jcp.2007.02.006.

Seifert, A., and K. D. Beheng, 2005: A two-moment cloud microphysics parameterization for mixed-phase clouds. part 1: Model description. *Meteorology and Atmospheric Physics*, **92 (1-2)**, 45–66, doi:https://doi.org/10.1007/s00703-005-0112-4.

Smith, P. L., C. G. Myers, and H. D. Orville, 1975: Radar reflectivity factor calculations in numerical cloud models using bulk parameterization of precipitation. *Journal of Applied Meteorology*, **14 (6)**, 1156–1165, doi:https://doi.org/10.1175/1520-0450(1975)014⟨1156:Rrfcin⟩2.0.Co;2.

Smithsonian, I., and R. J. List, 1951: Smithsonian meteorological tables. *Smithsonian Miscellaneous Collections*, **114 (1)**, 1–527.

Srivastava, R. C., 1967: A study of the effect of precipitation on cumulus dynamics. *Journal of the Atmospheric Sciences*, **24 (1)**, 36–45, doi:https://doi.org/10.1175/1520-0469(1967)024⟨0036:Asoteo⟩2.0.Co;2.

Stephens, G. L., and Coauthors, 2012: An update on earth's energy balance in light of the latest global observations. *Nature Geoscience*, **5 (10)**, 691–696, doi:https://doi.org/10.1038/Ngeo1580.

Stoelinga, M. T., 2005: *Simulated equivalent reflectivity factor as currently formulated in RIP: Description and possible improvements*.

Straka, J. M., 2009: *Cloud and Precipitation Microphysics*. Cambridge University Press, Cambridge, doi:https://doi.org/10.1017/cbo9780511581168.

Sun, Z., 2001: Reply to comments by greg m. mcfarquhar on 'parametrization of effective sizes of cirrus-cloud particles and its verification against observations'. (october b, 1999,125, 3037–3055). *Quarterly Journal of the Royal Meteorological Society*, **127 (571)**, 267–271, doi:https://doi.org/10.1002/qj.49712757116.

Sun, Z., and L. Rikus, 1999: Parametrization of effective sizes of cirrus-cloud particles and its verification against observations. *Quarterly Journal of the Royal Meteorological Society*, **125 (560)**, 3037–3055, doi:https://doi.org/10.1002/qj.49712556012.

Swann, H., 1998: Sensitivity to the representation of precipitating ice in crm simulations of deep convection. *Atmospheric Research*, **48**, 415–435, doi:https://doi.org/10.1016/S0169-8095(98)00050-7.

Tao, W.-K., and J. Simpson, 1993: Goddard cumulus ensemble model. parti: Model description. *Terrestrial, Atmospheric and Oceanic Sciences*, **4 (1)**, 35–71, doi:https://doi.org/10.3319/TAO.1993.4.1.35(A).

Thompson, G., R. M. Rasmussen, and K. Manning, 2004: Explicit forecasts of winter precipitation using an improved bulk microphysics scheme. part i: Description and sensitivity analysis. *Monthly Weather Review*, **132 (2)**, 519–542, doi:https://doi.org/10.1175/1520-0493(2004)132⟨0519:Efowpu⟩2.0.Co;2.

Tong, M. J., and M. Xue, 2005: Ensemble kalman filter assimilation of doppler radar data with a compressible nonhydrostatic model: Oss experiments. *Monthly Weather Review*, **133 (7)**, 1789–1807, doi:https://doi.org/10.1175/Mwr2898.1.

Trenberth, K. E., J. T. Fasullo, and J. Kiehl, 2009: Earth's global energy budget. *Bulletin of the American Meteorological Society*, **90 (3)**, 311–323, doi:https://doi.org/10.1175/2008bams2634.1.

REFERENCES

Van Weverberg, K., A. M. Vogelmann, H. Morrison, and J. A. Milbrandt, 2012: Sensitivity of idealized squall-line simulations to the level of complexity used in two-moment bulk microphysics schemes. *Monthly Weather Review*, **140 (6)**, 1883–1907, doi:https://doi.org/10.1175/mwr-d-11-00120.1.

Walko, R. L., W. R. Cotton, M. P. Meyers, and J. Y. Harrington, 1995: New rams cloud microphysics parameterization part i: the single-moment scheme. *Atmospheric Research*, **38 (1-4)**, 29–62, doi:https://doi.org/10.1016/0169-8095(94)00087-t.

Wallace, J. M., and P. V. Hobbs, 1977: *Atmospheric science : an introductory survey.* Academic Press, New York, xvii, 467 p. pp.

Wild, M., M. Z. Hakuba, D. Folini, P. Dorig-Ott, C. Schar, S. Kato, and C. N. Long, 2019: The cloud-free global energy balance and inferred cloud radiative effects: an assessment based on direct observations and climate models. *Clim Dyn*, **52 (7)**, 4787–4812, doi:https://doi.org/10.1007/s00382-018-4413-y.

Wyser, K., 1998: The effective radius in ice clouds. *Journal of Climate*, **11 (7)**, 1793–1802, doi:https://doi.org/10.1175/1520-0442(1998)011⟨1793:Teriic⟩2.0.Co;2.

Xu, K. M., and D. A. Randall, 1996: A semiempirical cloudiness parameterization for use in climate models. *Journal of the Atmospheric Sciences*, **53 (21)**, 3084–3102, doi:https://doi.org/10.1175/1520-0469(1996)053⟨3084:Ascpfu⟩2.0.Co;2.

Yau, M. K., and P. M. Austin, 1979: A model for hydrometer growth and evolution of raindrop size spectra in cumulus cells. *Journal of the Atmospheric Sciences*, **36 (4)**, 655–668, doi:https://doi.org/10.1175/1520-0469(1979)036⟨0655:Amfhga⟩2.0.Co;2.

Zhao, M., I. M. Held, S. J. Lin, and G. A. Vecchi, 2009: Simulations of global hurricane climatology, interannual variability, and response to global warming using a 50-km resolution gcm. *Journal of Climate*, **22 (24)**, 6653–6678, doi:https://doi.org/10.1175/2009jcli3049.1.

Zhao, Q. Y., and F. H. Carr, 1997: A prognostic cloud scheme for operational nwp models. *Monthly Weather Review*, **125 (8)**, 1931–1953, doi:https://doi.org/10.1175/1520-0493(1997)125⟨1931:Apcsfo⟩2.0.Co;2.

Zhou, L., S.-J. Lin, J.-H. Chen, L. M. Harris, X. Chen, and S. L. Rees, 2019: Toward convective-scale prediction within the next generation global prediction system. *Bulletin of the American Meteorological Society*, **100 (7)**, 1225–1243, doi:https://doi.org/10.1175/bams-d-17-0246.1.

Zhou, L., and Coauthors, 2015: Global energy and water balance: Characteristics from finite-volume atmospheric model of the iap/lasg (famil1). *Journal of Advances in Modeling Earth Systems*, **7 (1)**, 1–20, doi:https://doi.org/10.1002/2014ms000349.

Zhou, L., and Coauthors, 2022: Improving global weather prediction in gfdl shield through an upgraded gfdl cloud microphysics scheme. *Journal of Advances in Modeling Earth Systems*, **14 (7)**, e2021MS002 971, doi:https://doi.org/10.1029/2021MS002971.